IMMUNOLOGY

G-CSF secreted by mutant IDH1 glioma stem cells abolishes myeloid cell immunosuppression and enhances the efficacy of immunotherapy

**Mahmoud S. Alghamri[1,2], Brandon L. McClellan[1,2,3], Ruthvik P. Avvari[1,2], Rohit Thalla[1,2], Stephen Carney[1,2], Carson S. Hartlage[1,2], Santiago Haase[1,2], Maria Ventosa[1,2], Ayman Taher[1,2], Neha Kamran[1,2], Li Zhang[1,2], Syed Mohd Faisal[1,2], Felipe J. Núñez[1,2†], María Belén Garcia-Fabiani[1,2], Wajd N. Al-Holou[1], Daniel Orringer[1‡], Shawn Hervey-Jumper[4], Jason Heth[1], Parag G. Patil[1], Karen Eddy[1], Sofia D. Merajver[5], Peter J. Ulintz[5§], Joshua Welch[6], Chao Gao[6], Jialin Liu[6], Gabriel Núñez[7], Dolores Hambardzumyan[8], Pedro R. Lowenstein[1,2,9], Maria G. Castro[1,2,9]*

Mutant isocitrate-dehydrogenase 1 (*mIDH1*) synthesizes the oncometabolite 2-hydroxyglutarate (2HG), which elicits epigenetic reprogramming of the glioma cells' transcriptome by inhibiting DNA and histone demethylases. We show that the efficacy of immune-stimulatory gene therapy (TK/Flt3L) is enhanced in *mIDH1* gliomas, due to the reprogramming of the myeloid cells' compartment infiltrating the tumor microenvironment (TME). We uncovered that the immature myeloid cells infiltrating the *mIDH1* TME are mainly nonsuppressive neutrophils and pre-neutrophils. Myeloid cell reprogramming was triggered by granulocyte colony-stimulating factor (G-CSF) secreted by *mIDH1* glioma stem/progenitor-like cells. Blocking G-CSF in *mIDH1* glioma–bearing mice restores the inhibitory potential of the tumor-infiltrating myeloid cells, accelerating tumor progression. We demonstrate that G-CSF reprograms bone marrow granulopoiesis, resulting in noninhibitory myeloid cells within *mIDH1* glioma TME and enhancing the efficacy of immune-stimulatory gene therapy.

INTRODUCTION

Mutation in isocitrate dehydrogenase (*mIDH*) is a common genetic lesion in glioma patients (*1*). Approximately 90% of *IDH1* mutations occur in exon 4 at codon 132, resulting in a change of a single amino acid from arginine to histidine (R132H). Less common *IDH2* mutations occur in an analogous codon at position R172 (*2*). Although IDH1/2 mutations are always heterozygous, they exert a dominant gain-of-function enzymatic activity, which leads to the production of 2-hydroxyglutarate (2HG). Excessive 2HG production causes DNA hypermethylation via inhibition of methylcytosine dioxygenase *TET2* (*3*) and also promotes histone hypermethylation through competitive inhibition of α-ketoglutarate (αKG)–dependent Jumonji-C histone demethylases (*4*). This leads to epigenetic reprogramming of the transcriptome within the *mIDH1* glioma cells (*4*, *5*).

Several studies suggested that *mIDH1* may play a critical role in shaping the immunological landscape of the tumor microenvironment (TME) (*6*–*9*). Glioma samples from patients with *mIDH1* have decreased Programmed death-ligand 1 (PD-L1) expression (due to hypermethylation of the CD274 promoter) (*7*, *10*), reduced levels of inflammation, and reduced levels of infiltrating immune cells (*6*, *8*). Myeloid cells represent the major immune cells infiltrating the glioma microenvironment (*11*, *12*). It has recently been shown that the TME, from a genetically engineered mouse model (GEMM) of *mIDH1* glioma (*PDGFB/shP53/Ink4a/Arf*$^{-/-}$*/mIDH1*), exhibits fewer tumor-infiltrating macrophages, dendritic cells (DCs), and neutrophils compared to the wild-type *IDH1* counterpart (*6*). Nevertheless, the impact of *mIDH1* on tumor-infiltrating myeloid cells' phenotype and function, as well as the impact of *mIDH1* in glioma on the response to immunotherapies, has not been explored, particularly in the context of concurrent inactivation mutations in *ATRX* and *TP53* (*1*, *13*).

In this context, the lack of therapeutic efficacy of immunotherapies in patients with glioma in the clinical arena can be attributed, in part, to the immunosuppressive properties elicited by glioma-infiltrating immune cells (*14*). Myeloid-derived suppressor cells (MDSCs) have emerged as one of the dominant types of immunosuppressive cells that directly interfere with the efficacy of immunotherapy (*12*, *15*). In patients with glioma, it has been demonstrated that granulocytic MDSCs [also known as polymorphonuclear (PMN)–MDSCs] are a major subset that expand during glioma progression, which negatively correlates with patients' survival (*16*–*18*).

Here, we demonstrate that gliomas harboring *mIDH1* in the context of *ATRX* and *TP53* deficiency exhibit an enhanced therapeutic response to immune-stimulatory gene therapy (herpes simplex virus 1–thymidine kinase/Feline McDonough sarcoma (Fms)–like tyrosine kinase 3 ligand: TK/Flt3L) when compared to *wtIDH1* tumors. MDSC depletion enhanced TK/Flt3L therapeutic efficacy in *wtIDH1* glioma– but not in *mIDH1* glioma–bearing mice. We report that in genetically engineered *mIDH1* glioma mouse models, there is an expansion of tumor-infiltrating granulocytes when compared to

[1]Department of Neurosurgery, University of Michigan Medical School, Ann Arbor, MI 48109, USA. [2]Department of Cell and Developmental Biology, University of Michigan Medical School, Ann Arbor, MI 48109, USA. [3]Graduate Program in Immunology, University of Michigan Medical School, Ann Arbor, MI 48109, USA. [4]Department of Neurosurgery, University of California San Francisco, San Francisco, CA 94143, USA. [5]Department of Internal Medicine, University of Michigan Medical School, Ann Arbor, MI 48109, USA. [6]Department of Computational Medicine and Bioinformatics, University of Michigan Medical School, Ann Arbor, MI 48109, USA. [7]Department of Pathology, University of Michigan Medical School, Ann Arbor, MI 48109, USA. [8]Department of Oncological Sciences, The Tisch Cancer Institute, and Department of Neurosurgery, Icahn School of Medicine at Mount Sinai, New York, NY 10029, USA. [9]Rogel Cancer Center, University of Michigan, Ann Arbor, MI 48109, USA.
*Corresponding author. Email: mariacas@umich.edu
†Present address: Leloir Institute Foundation, Buenos Aires, Argentina.
‡Present address: Department of Neurosurgery, New York University, New York, NY 10018, USA.
§Present address: Diamond Age Data Science, 26 Ivaloo St, Somerville, MA 02143, USA.

wtIDH1 glioma. Upon phenotypic and functional characterization, we uncovered that tumor-infiltrating granulocytes in *mIDH1* glioma, counter to the tumor-infiltrating granulocytes in *wtIDH1*, did not exhibit immune-suppressive properties. Single-cell sequencing coupled with mass cytometry analysis revealed that these granulocytes are heterogeneous and composed of three distinct clusters, i.e., neutrophils, preneutrophils, and a smaller cluster of bona fide immunosuppressive PMN-MDSCs. Moreover, primary human gliomas showed a higher frequency of cells exhibiting the PMN-MDSC gene signature in *wtIDH1* tumors when compared to *mIDH1* glioma. Our data demonstrate that the mechanism by which *mIDH1* in glioma mediates the expansion of nonimmunosuppressive granulocytes involves epigenetic reprogramming. This leads to enhanced expression of granulocyte colony-stimulating factor (G-CSF) by stem-like *mIDH1* glioma cells. Blocking G-CSF restored the inhibitory potential of PMN-MDSCs and accelerated tumor progression. Our results also demonstrate that systemic administration of recombinant G-CSF (rG-CSF) prolonged the median survival (MS) of *wtIDH1* glioma–bearing mice and rendered tumor-infiltrating MDSCs nonimmunosuppressive. Consistent with that, low-grade glioma (LGG) astrocytoma with *mIDH1* is the sole tumor cohort within all The Cancer Genome Atlas (TCGA) datasets in which high *CSF3* gene expression correlates with favorable patients' outcome. Our data provide mechanistic insights related to the impact of *mIDH1* on the phenotypic and functional properties of myeloid cells in the glioma TME. This study reveals an important role of *mIDH1* on reprogramming the phenotypic and functional diversity of myeloid cells in glioma TME, a feature that can be harnessed to enhance the efficacy of immunotherapies in patients with glioma.

RESULTS

Immune stimulatory gene therapy eradicates *mIDH1* tumor irrespective of Ly6G$^+$ myeloid cell depletion

The role of *IDH1* mutation in shaping the immune landscape and response to immunotherapy in glioma is poorly understood. We have recently shown that the PMN-MDSCs are the major immune cells infiltrating the high-grade glioma with *wtIDH1*, and they determine the efficacy of immunotherapy (*12*). To uncover the impact of $IDH1^{R132H}$ in the context of *ATRX* and *TP53* deficiency on glioma-infiltrating PMN-MDSCs and the response to immunotherapy, we generated a *mIDH1* GEMM using the Sleeping Beauty (SB) transposon system (*19*–*21*). Two groups of implantable neurospheres were generated using the SB method; each contains a combination of genetic lesions commonly encountered in astrocytoma: the *mIDH1* group [*shp53*/*shATRX*/$mIDH1^{R132H}$ (NPAI)] and the control *wtIDH1* group [*shp53*/*shATRX*/*wtIDH1* (NPA)] (fig. S1A). Similar to the human data, the *mIDH1* tumor–bearing mice have a longer MS compared to the *wtIDH1* group [*wtIDH1* MS = 21 days postimplantation (dpi) and *mIDH1* MS = 33 dpi] (fig. S1B). Using this model, we tested the efficacy of immune stimulatory gene therapy TK/Flt3L that induces a robust antitumor T cell response leading to tumor regression, long-term survival, and immunological memory in glioblastoma models (*12*, *22*) (Fig. 1A). The efficacy of TK/Flt3L in *mIDH1* was tested in combination with PMN-MDSC depletion using the αLy6G antibody. The depletion was timed to coincide with the peak of TK/Flt3L-induced T cell response occurring at ~7 days after immune-mediated gene therapy (Fig. 1B) (*12*, *22*, *23*). Administration of α Lymphocyte antigen 6 complex locus G6D (Ly6G) antibody as monotherapy to *wtIDH1* or *mIDH1* glioma–bearing mice did not confer survival benefit (Fig. 1, C and D). However, treatment *wtIDH1* tumor–bearing mice with TK/Flt3L significantly prolonged their survival ($P < 0.05$; Fig. 1C). Unexpectedly, TK/Flt3L gene therapy resulted in a much greater survival benefit in the *mIDH1* tumor–bearing animals as compared to those with *wtIDH1* tumor (Fig. 1D). Approximately 85% of *mIDH1* tumor–bearing animals survived long term when treated with TK/Flt3L gene therapy (Fig. 1D). Combining TK/Flt3L gene therapy with Ly6G depletion confers survival benefit in the *wtIDH1* but not in the *mIDH1* tumor–bearing mice ($P < 0.05$; Fig. 1, C and D). We confirmed the tumor eradication in the *mIDH1* groups treated with either TK/Flt3L + isotype or TK/Flt3L + αLy6G by hematoxylin and eosin staining, which showed no signs of tumor in the long-term survivors (Fig. 1F). In contrast, the *mIDH1* groups treated with saline or saline + αLy6G displayed tumor burden (Fig. 1F). To test whether these mice developed an immunological memory response, we rechallenged the long-term survivors from the TK/Flt3L + isotype and TK/Flt3L + αLy6G groups with *mIDH1* mouse neurospheres implanted in the contralateral hemisphere at day 90 after initial tumor implantation (Fig. 1G). These animals remained tumor free without further treatment, whereas control mice implanted with *mIDH1* neurospheres succumbed because of tumor burden (Fig. 1H). These results validate the effectiveness of TK/Flt3L against *mIDH1* tumors regardless of myeloid cell depletion. We concluded that glioma harboring *mIDH1* exhibit an improved response to immunotherapy and that Ly6G depletion does not improve the therapeutic response to TK/Flt3L.

Depletion of myeloid cells in combination with immunotherapy enhances antitumor CD8 T cell response in *wtIDH1* but not in *mIDH1* glioma

To provide a mechanistic basis for the different responses to immunotherapy observed in our glioma models, we examined the effect of PMN-MDSC depletion in combination with immune-stimulatory TK/Flt3L gene therapy in *wtIDH1* and *mIDH1* model harboring the surrogate tumor antigen, ovalbumin (OVA). We sought to examine the impact of treatment on the quantity and quality of the antitumor T cell response (fig. S1C). Using OVA expressing *wtIDH1* or *mIDH1* neurospheres, we were able to quantify tumor-specific CD8$^+$ T cells by making use of the SIINFEKL-H2Kb expressing CD8$^+$ T cells. TK/Flt3L treatment increased the frequency of total CD8$^+$ T cells infiltrating both *wtIDH1* and *mIDH1* glioma, with no differences between isotype or Ly6G depletion (fig. S1, D and E). Combining TK/Flt3L with Ly6G depletion increased the frequency of tumor-specific CD8$^+$ T cells in the TME (~1.6-fold) compared to the TK/Flt3L + isotype ($P < 0.05$) in the *wtIDH1* group but not in the *mIDH1* group (Fig. 1E). The *mIDH1* tumor–bearing mice showed more than twofold increase in the percentage of tumor-specific T cells in response to the gene therapy (TK/Flt3L) with no difference between the Ly6G depletion and control (Fig. 1E).

To test the impact of PMN-MDSCs on the cytotoxicity of CD8$^+$ T cells in the TME, we investigated the granzyme B (GzB) expression in CD8$^+$ T cells. TK/Flt3L gene therapy resulted in a more than twofold increase in the frequency of GzB$^+$ CD8$^+$ T cells compared to saline-treated animals (fig. S1, F and G). This was further enhanced in the presence of Ly6G depletion in *wtIDH1* but not in the *mIDH1* group (fourfold, $P < 0.05$; fig. S1, F and G). Overall, these data suggest that *mIDH1* tumors have an enhanced response to immunotherapies

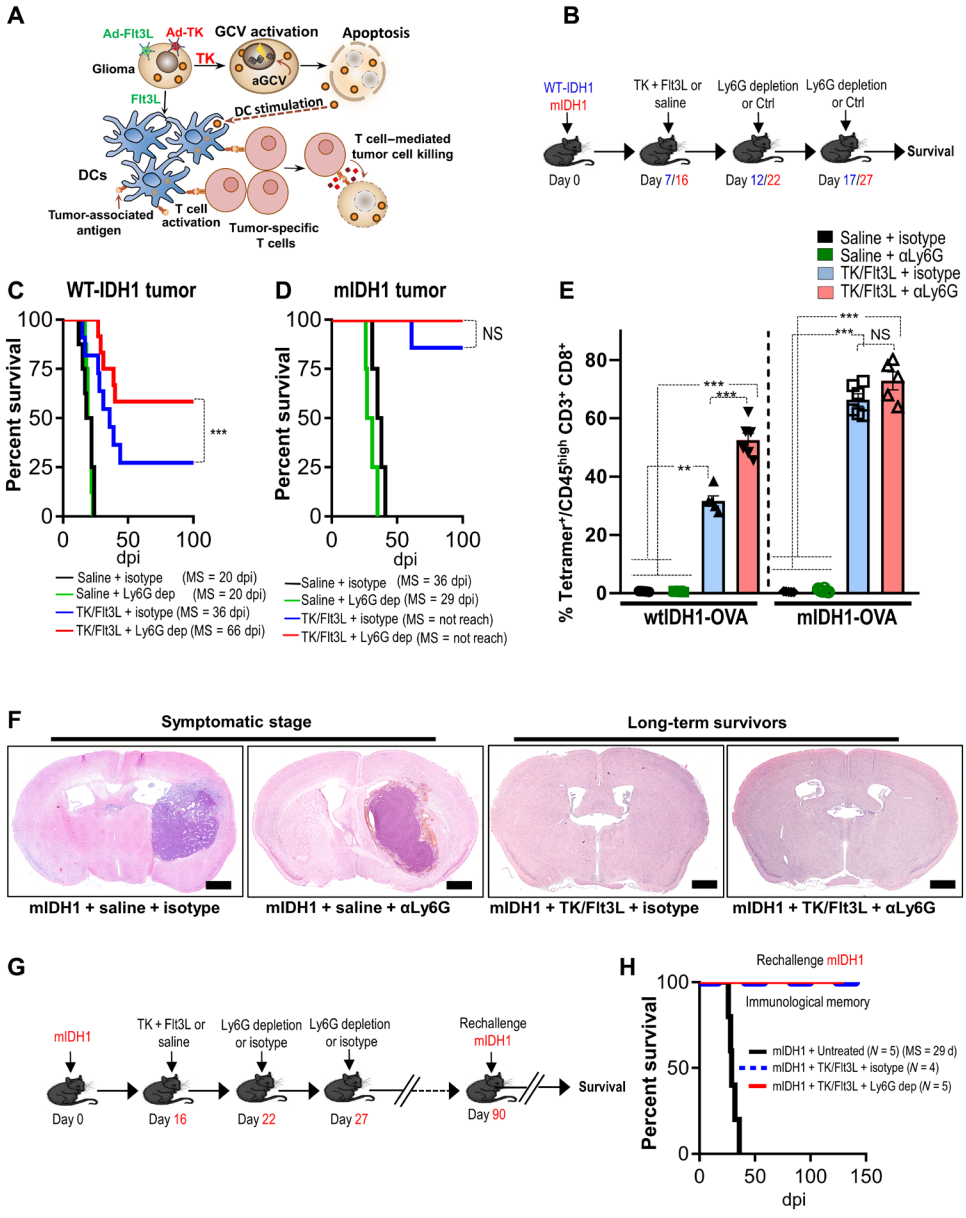

Fig. 1. *mIDH1* tumor models have enhanced response to immune-stimulatory gene therapy irrespective of myeloid cell depletion. (**A**) Schematic showing the mechanism by which TK/Flt3L gene therapy recruits and activates a tumor-specific T cell response. (**B**) Schematic illustrating the treatment strategy of the TK + Flt3L gene therapy in combination with Ly6G depletion in *wtIDH1* or *mIDH1* tumor–bearing mice. WT, wild type. (**C** and **D**) Kaplan-Meier survival curves of implanted mice-bearing *wtIDH1* or *mIDH1* tumors, treated with TK + Flt3L, Ly6G depletion, or combination therapy. dpi, days postimplantation; NS, not significant. (**E**) Tumor-specific CD8 T cell frequency within the TME of *wtIDH1* or *mIDH1* tumors treated with TK + Flt3L, Ly6G depletion, or combination therapy was analyzed by staining for SIINFEKL-Kb tetramers. (**F**) Hematoxylin and eosin staining of brain sections from *mIDH1* tumors treated with saline, αLy6G, TK/Flt3L, and TK/Flt3L + αLy6G. (**G**) Schematic illustrating the treatment strategy of the TK + Flt3L gene therapy in combination with Ly6G depletion in *mIDH1* tumor–bearing mice. Most *mIDH1* tumor–bearing mice (90%) survived long term in response to TK/Flt3L gene therapy regardless of Ly6G depletion. The long-term survived mice were rechallenged at day 90 after implantation. (**H**) Kaplan-Meier survival plot for rechallenged long-term survivors from *mIDH1* + TK/Flt3L + isotype ($N = 4$), *mIDH1* + TK/Flt3L + Ly6G dep ($N = 5$), or control (*mIDH1* + untreated) ($N = 5$). Data were analyzed using the log-rank (Mantel-Cox) test. Scale bars, 1 mm. $^{**}P < 0.01$ and $^{***}P < 0.005$, One-way analysis of variance (ANOVA).

regardless of Ly6G depletion, suggesting an altered functional property of the PMN-MDSCs infiltrating the *mIDH1* glioma.

mIDH1 glioma in the context of *ATRX and TP53* inactivation causes expansion of the granulocytic myeloid cells

To study the impact of *mIDH1* on the phenotype of myeloid cells, we used the merit of mass cytometry by time of flight (CyTOF) (table S1), which measures 37 parameters simultaneously, to analyze immune cell composition within the TME. Using Spanning-tree progression analysis for density-normalized events (SPADE) analysis (*24*), we found that the glioma TME contains several immune cell types including macrophages, DCs, B cells, natural killer (NK) cells, $CD8^+$ T cells, and $CD4^+$ T cells (Fig. 2, A and B). There was an expansion of cells (depicted by the large red/yellow nodes) characteristic

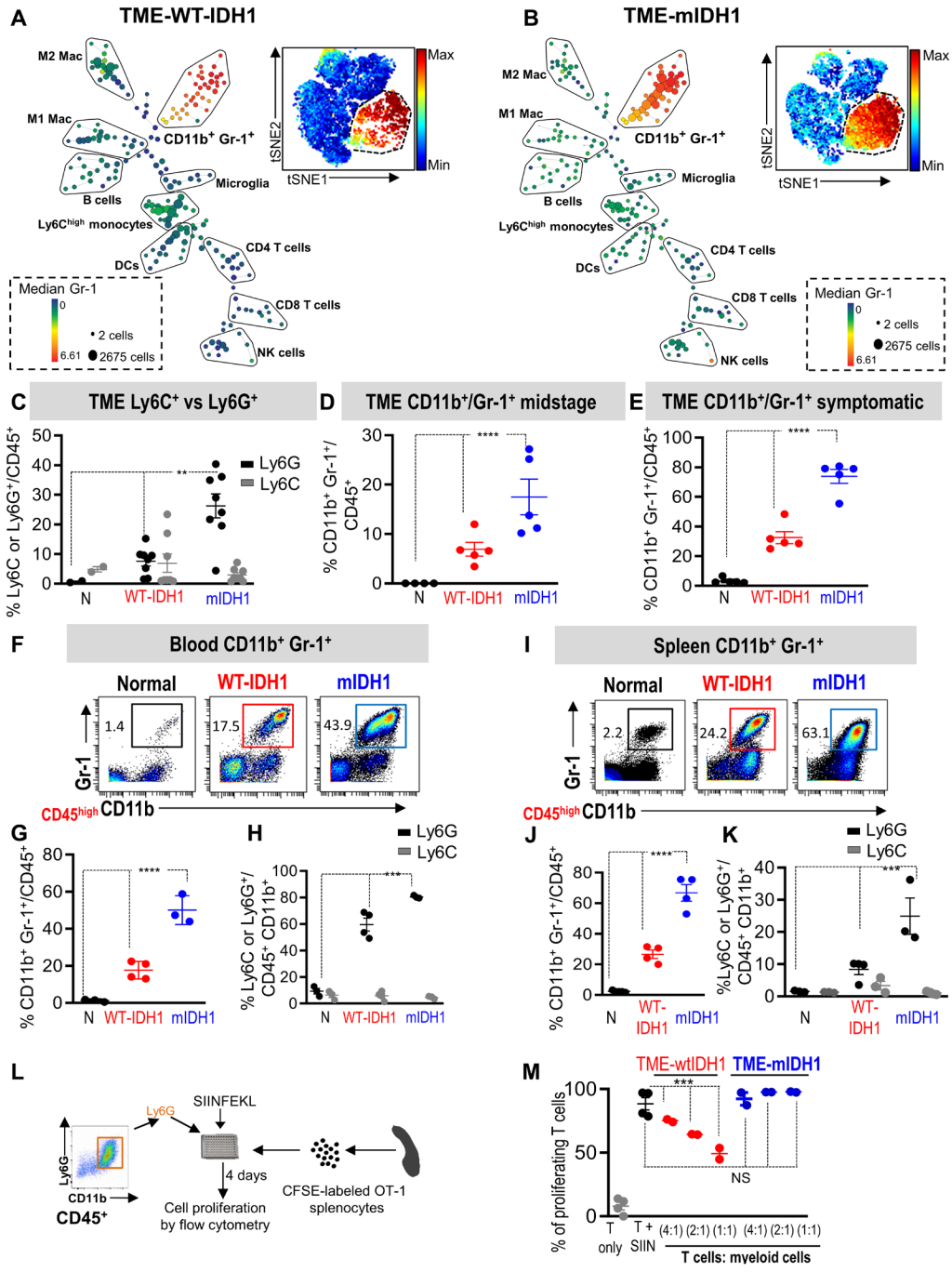

Fig. 2. *mIDH1* glioma models have high expansion of granulocytic myeloid cell population ($CD45^{high}/CD11b^{+}/Ly6G^{+}$). (**A** and **B**) SPADE analysis of mass cytometry (CyTOF) data represents immune cell composition within the TME of SB-induced *wtIDH1* (A) or *mIDH1* (B) tumors. Insets are viSNE visualizations of high-dimensional mass cytometry data; color intensity represents the Gr-1 expression level. (**C**) Phenotypic characterization of $CD45^{high}/CD11b^{+}/Gr\text{-}1^{+}$ population as granulocytic or monocytic based on the expression of Ly6G or Ly6C at symptomatic stage. Most of the $CD45^{high}/CD11b^{+}/Gr\text{-}1^{+}$ in the *mIDH1* glioma TME are $CD45^{high}/CD11b^{+}/Ly6G^{+}$ (granulocytic) cells. (**D** and **E**) Flow cytometry analysis of the frequency of MDSCs ($CD45^{high}/CD11b^{+}/Gr\text{-}1^{+}$) within the TME at the midstage of tumor implantation (D) and at the symptomatic stage (E). The percentage of $CD45^{high}/CD11b^{+}/Gr\text{-}1^{+}$ cells was higher in *mIDH1* tumors compared to *wtIDH1* tumors. (**F** and **G**) CyTOF analysis of $CD45^{high}/CD11b^{+}/Gr\text{-}1^{+}$ cells in blood from mice with no tumor (normal) and SB-induced *wtIDH1* or *mIDH1* glioma. (**H**) Phenotypic characterization of circulating $CD45^{high}/CD11b^{+}/Gr\text{-}1^{+}$ cells according to expression of Ly6C or Ly6G. (**I** and **J**) CyTOF analysis of $CD45^{high}/CD11b^{+}/Gr\text{-}1^{+}$ cells from the spleens of mice with no tumor and SB-induced *wtIDH1* or *mIDH1* glioma. (**K**) Phenotypic characterization of splenic $CD45^{high}/CD11b^{+}/Gr\text{-}1^{+}$ cells according to expression of Ly6C or Ly6G. (**L**) Schematic figure of the in vitro T cell proliferation assay. (**M**) Flow analysis of the inhibitory potential of $CD45^{high}/CD11b^{+}/Ly6G^{+}$ cells from TME of *wtIDH1* or *mIDH1* tumor. N = normal, $^{**}P < 0.01$, $^{***}P < 0.005$, and $^{****}P < 0.0001$, ANOVA.

for MDSCs ($CD45^{high}/CD11b^{+}/Gr\text{-}1^{+}$) in the TME of *mIDH1* glioma compared to *wtIDH1* glioma (Fig. 2, A and B). Similarly, visual inspection of viSNE plots, which represent high-dimensional CyTOF output in two dimensions (*25*), showed a higher percentage of $Gr\text{-}1^{+}$ cells in the TME from *mIDH1* glioma compared to those from *wtIDH1* glioma (Fig. 2, A and B, insets).We confirmed that this difference is statistically significant using a χ^2 test ($P < 0.0001$). The Gr-1 antibody can detect both the granulocytic ($CD45^{high}/CD11b^{+}/Ly6G^{+}/Ly6C^{low}$) and monocytic ($CD45^{high}/CD11b^{+}/Ly6G^{-}/Ly6C^{high}$) MDSC populations. We found that most of the expanded myeloid cell populations in the *mIDH1* tumor belonged to the granulocytic population, with no changes in the frequency of the monocytic population (Fig. 2C). To further validate the abundance of the Ly6G population in the TME of the *mIDH1* tumor, we used the CITRUS algorithm (cluster identification, characterization, and regression) to identify abundant populations in *wtIDH1* versus *mIDH1* tumors (*26*). The relative frequencies of these clustered populations were compared between the two groups. Results showed that two major node clusters were different between the TME from *wtIDH1* versus the TME from *mIDH1* (fig. S2A; red nodes). The first population expresses mainly Ly6G, which was abundant in the *mIDH1* group (clusters 1 to 9) (fig. S2, B to K). In contrast, the TME from *wtIDH1* tumors has higher abundance of macrophage clusters (clusters 12, 27, and 17 to 25) (fig. S3, A to M). These results showed that the *mIDH1* tumors have a higher frequency of granulocytic myeloid cells but a lower frequency of macrophages.

In addition to the increase in granulocytes, *mIDH1* tumors showed a decreased frequency of DCs (~4-fold) with no significant change in the frequency of lymphocytes (including NK cells, B cells, and $CD8^{+}$ and $CD4^{+}$ T cells) as compared to *wtIDH1* tumors (fig. S4, A to H). Notably, there was no significant difference in the percentage of $CD45^{+}$ cells between *wtIDH1* and *mIDH1* glioma (fig. S4H). To test whether the increase in myeloid cells is associated with the tumor growth, we analyzed the frequency of $CD45^{high}/CD11b^{+}/Gr\text{-}1^{+}$ population at the midstage (12 days after implantation) and at the symptomatic stage of tumor development (Fig. 2, D and E). In both time points, we found that the *mIDH1* tumor group had an increased frequency of $CD45^{high}/CD11b^{+}/Gr\text{-}1^{+}$ cells compared to the *wtIDH1* group (Fig. 2, D and E).

The expansion of $CD45^{high}/CD11b^{+}/Ly6G^{+}$ cells was not limited to the tumor site; in both the circulation and the spleen of *mIDH1* tumor–bearing animals, there was a higher number and percentage of $CD45^{high}/CD11b^{+}/Ly6G^{+}$ (Fig. 2, F to K, and figs. S5 and S6). Moreover, in both the circulation and spleen from tumor-bearing animals, there was no significant difference in the M-MDSCs between *wtIDH1* and *mIDH1* glioma–bearing mice (figs. S5 and S6). However, *mIDH1* exhibited a decreased number of macrophages in the circulation and spleen, with no differences in the DCs or lymphocytes (figs. S5 and S6).

We validated our findings using two additional glioma mouse models. First, we used the glioma model induced by Replication-Competent Avian leukemia virus Splice acceptor expressing platelet-derived growth factor β (*PDGFB*), *shTP53*, and *mIDH1* or *wtIDH1* in *NTva_Ink4a/Arf*$^{-/-}$ mice (*19*, *27*). Neurospheres cultured from these tumors were engineered to encode *shATRX*, as described in Materials and Methods, to generate glioma cells with the following molecular alterations: *PDGFB/shTP53/shATRX/Ink4a/Arf*$^{-/-}$*/mIDH1* or *PDGFB/shTP53/shATRX/Ink4a/Arf*$^{-/-}$*/wtIDH1* (*19*). Second, we used the SB-generated mouse model that harbors the following genetic lesions: *CDKN2A*$^{-/-}$*/shP53/shATRX/wtIDH1* (CPA) or *CDKN2A*$^{-/-}$*/shP53/shATRX/mIDH1* (CPAI). In both models, we confirmed that the *mIDH1* tumor–bearing animals exhibit an expanded $CD45^{high}/CD11b^{+}/Gr\text{-}1^{+}$ population with a high predominance of the $CD45^{high}/CD11b^{+}/Ly6G^{+}$ population (fig. S7). Collectively, these results suggest that the *mIDH1* tumor causes activation of pathways favoring granulocytic myeloid cells' expansion.

Granulocytic myeloid cells infiltrating *mIDH1* glioma are not immunosuppressive

Immunosuppressive $CD45^{high}/CD11b^{+}/Ly6G^{+}$ cells are characterized by their ability to suppress T cell functions. Therefore, we examined the influence of tumor-infiltrating $CD45^{high}/CD11b^{+}/Ly6G^{+}$ myeloid cells on antigen-specific T cell proliferation. We isolated granulocytes by flow cytometry from gliomas expressing *wtIDH1* or *mIDH1* and cocultured them with carboxyfluorescein diacetate succinimidyl ester (CFSE)–labeled splenocytes from OT-1 mice (Fig. 2L). Isolated splenocytes were stimulated with the cognate OVA peptide, SIINFEKL (SIIN), to induce OT-1–specific T cell proliferation (Fig. 2L). In response to SIIN, T cell proliferation spiked to ~90% in the control condition (T + SIIN) (Fig. 2M). When $CD45^{high}/CD11b^{+}/Ly6G^{+}$ myeloid cells from the TME of *wtIDH1* tumors were added to the culture at different ratios (T cells:myeloid cells; 1:1, 2:1, and 4:1), the percentage of proliferating T cells was reduced to ~48, 64, and 75%, respectively (Fig. 2M). Unexpectedly, $CD45^{high}/CD11b^{+}/Ly6G^{+}$ cells isolated from the TME of *mIDH1* gliomas failed to suppress antigen-specific T cell proliferation at any coculturing ratio (Fig. 2M). The effect of *mIDH1* on the function of tumor-infiltrating $CD45^{high}/CD11b^{+}/Ly6G^{+}$ cells was validated using the two additional mouse models described above. In both models, we found that $CD45^{high}/CD11b^{+}/Ly6G^{+}$ cells isolated from the *mIDH1* TME do not inhibit T cell proliferation (fig. S8). Notably, granulocytes isolated from spleens of *wtIDH1* or *mIDH1* tumor–bearing mice failed to inhibit antigen-specific T cell proliferation (fig. S9). Together, these results suggest that the expanded granulocytes in *mIDH1* TME are not inhibitory. To further investigate the effect of granulocytes on T cell activation, we isolated T cells from the spleen of tumor-free mice and incubated them with beads loaded with anti-CD3 and anti-CD28 (Dynabeads) (fig. S10A). Tumor-infiltrating $CD11b^{+}/Ly6G^{+}$ myeloid cells isolated from *wtIDH1* or *mIDH1* tumors were added to the culture, and T cell activation was analyzed by CD69 expression (fig. S10A). Results showed that granulocytes from *wtIDH1* markedly decreased CD69 expression in a ratio-dependent manner, whereas the granulocytes from *mIDH1* did not change CD69 expression in $CD8^{+}$ T cells at any coculturing ratio (fig. S10, B to E).

To investigate whether a tumor-derived factor is responsible for remodeling granulocytes in *mIDH1*, we performed an ex vivo MDSC differentiation assay. We isolated bone marrow (BM) cells from naïve mice and cultured them in media containing 10% fetal bovine serum (FBS), with *wtIDH1* neurospheres or with *mIDH1* neurospheres (2:1, BM cells:neurospheres) (fig. S11A). After 7 days, we analyzed the frequency of granulocytes formed in each condition (fig. S11A). Consistent with the in vivo data, there was a higher percentage of $CD45^{high}/CD11b^{+}/Ly6G^{+}$ cells expressing lower levels of Arg1, PD-L1, and CD80 in the *mIDH1* coculture condition (fig. S11, B to E). In contrast to granulocytes generated from *wtIDH1* coculture, $CD45^{high}/CD11b^{+}/Ly6G^{+}$ cells generated from *mIDH1* culture failed to inhibit antigen-specific T cell proliferation in vitro (fig. S11, F and G). Collectively, these data validate that a tumor-derived factor

is responsible for developing the nonimmunosuppressive myeloid cells in *mIDH1* glioma.

mIDH1 glioma development results in profound remodeling of BM hematopoiesis

The expansion of the granulocytic myeloid cells within the TME, blood, and spleen suggested that *mIDH1* tumor growth induces profound alterations in the BM hematopoiesis. Therefore, we examined the changes in hematopoiesis within the BM and spleen of the SB-induced murine glioma model. We found that within the lin$^-$ population, the frequency of LSK (Lin$^-$/c-Kit$^+$/Sca-1$^+$) was decreased in the BM from *mIDH1* tumor–bearing mice (2.2-fold, $P < 0.05$; Fig. 3, A and B). In contrast, BM from *mIDH1* tumors contained higher frequencies of myeloid progenitors (MPs; %MP ~13%, $P < 0.05$;Fig. 3, A and C). In the spleen, there were no differences in the frequency of LSK between the *wtIDH1* and *mIDH1* tumor–bearing animals (Fig. 3, I and J). However, spleens from *mIDH1* tumor–bearing animals showed more than twofold increase in MPs compared to *wtIDH1* tumors ($P < 0.05$; Fig. 3, I and K). There was also a higher frequency (twofold) of granulocyte-macrophage precursors (GMPs) in both the BM and spleen of *mIDH1* tumor–bearing animals ($P < 0.05$, Fig. 3, E, F, L, and M). Despite the increase in MPs and GMPs, there was no significant change in the frequency of common lymphocyte progenitors (CLPs) between the two groups (Fig. 3, G, H, N, and O). The enhanced production of granulocytes, MPs, and GMPs in BM and spleen indicates the activation of the granulocytic myeloid differentiation pathway in *mIDH1* tumor–bearing animals (Fig. 3D).

Molecular and phenotypic characterization of *mIDH1* tumor–infiltrating granulocytes

We next investigated the molecular characteristics of the expanded CD45^{high}/CD11b$^+$/Ly6G$^+$ cells in *mIDH1* tumors. First, we examined the surface expression of T cell–suppressive/costimulatory molecules commonly expressed by PMN-MDSCs. In the CD45^{high}/CD11b$^+$/Ly6G$^+$ cells from *mIDH1* TME, the expression level of immunosuppressive and costimulatory molecules, such as PD-L1, CD86, CD80, interleukin-4Rα (IL-4Rα), inducible nitric oxide synthase, and arginase 1, was lower compared to these within *wtIDH1* TME (Fig. 3, P to U). To characterize the molecular differences between *mIDH1* and *wtIDH1* tumor–infiltrating myeloid cells, we purified CD45^{high}/CD11b$^+$/Gr-1$^+$ cells from tumor-bearing animals and performed transcriptome analysis. Compared to *wtIDH1*, myeloid cells isolated from *mIDH1* tumors have decreased expression of all immunosuppressive genes associated with the PMN-MDSC signature, such as *Il1β*, *Arg1*, *Tgfb1*, *CD274*, and *Stat3* (Fig. 3V).

Single-cell transcriptome analysis reveals that neutrophils and preneutrophils are the major granulocytic lineages in *mIDH1* TME

To compare the molecular differences of TME-derived granulocytes on an individual cell basis, we used single-cell RNA sequencing (scRNA-seq) coupled with mass cytometry (Fig. 4A). Two biological replicates of purified immune cells from TME of *mIDH1* mice (8881 cells) and TME of *wtIDH1* mice (7408 cells) were sequenced at an average depth of ~20,000 reads per cell. After filtering cells with low overall expression and/or high mitochondrial gene expression, we performed dimensionality reduction and unsupervised cell clustering, using methods implemented in the Seurat software suite, independently for *mIDH1* and *wtIDH1* datasets to identify distinct cell populations (*28*) (fig. S12, A and B). In *mIDH1* tumors, we identified 14 distinct cell clusters expressing known markers of major immune cell types (Fig. 4B). Granulocytes formed the largest population and consisted of three clusters, which we refer to as C1, C2, and C3 (Fig. 4B and fig. S12, B and D). C1 displayed high expression of PMN-MDSC–related genes such as *Il1*b and *Arg2*, two major immunosuppressive factors previously used to define PMN-MDSCs in cancer models (*29*) (Fig. 4C and fig. S12, B and D). C2 constitutes the largest granulocytic cluster and expressed high levels of *S100a8*, inflammatory cytokines involved in the recruitment of CD8$^+$ T cells (*Ccl3* and *Ccl4*), and cell cycle genes such as *Cdc20* and *G0s2* (fig. S12D) (*30*). C3 expressed genes involved in neutrophil maturation (*Cebpe* and *Mpo*; Fig. 4C and fig. S12D). These results suggest that C1 belongs to the immunosuppressive PMN-MDSC population within the TME of *mIDH1* tumors, whereas C2 and C3 correspond to preneutrophils and neutrophils, respectively. In *wtIDH1*, there was only one cluster of granulocytes (C7; fig. S12, A and C). This cluster expressed PMN-MDSC–related genes such as *Il1*b and *Arg2*, similar to cluster C1 in TME-*mIDH1* (Fig. 4C and fig. S12, A and C).

To confirm that granulocytes in *wtIDH1* tumor (C7) are similar to C1 granulocytes in the *mIDH1* tumor, we integrated the *wtIDH1* and *mIDH1* tumor–infiltrating immune cell datasets using functionality available in the Seurat package (*31*). Jointly clustering *wtIDH1* and *mIDH1* tumor–infiltrating immune cells showed that the granulocytic population formed three clusters corresponding to the C1, C2, and C3 clusters found in the TME of *mIDH1* tumors (fig. S13, A to C). Most of the granulocytes from the TME of the *wtIDH1* tumor clustered with the C1 cluster of granulocytes from *mIDH1* tumors (fig. S13, B to D), suggesting that these cells share a common origin and have a similar function.

To further determine whether C1 represents the immunosuppressive PMN-MDSCs within TME-*mIDH1*, we looked for a cell surface marker differentially expressed in C1 that would allow us to isolate cells belonging to this cluster and assess their function. Among the top 50 differentially expressed genes in cluster C1, *CD274* (PD-L1) was the only cell surface marker that showed high expression in C1 compared to moderate and low expression in C2 and C3, respectively (Fig. 4C and table S4). On the basis of *CD274* expression, we reclassified the granulocytic populations of both TMEs. We found that there was one granulocyte population in the *wtIDH1* tumors and three distinct granulocytic populations in the *mIDH1* tumors, corresponding to C1, C2, and C3 (Fig. 4, D and E). We FACS (fluorescence-activated cell sorting)–sorted each population based on the expression of PD-L1 (see fig. S14 for gating strategy) and determined their inhibitory potential by performing a T cell proliferation assay. Similar to the results obtained with granulocytes from *wtIDH1* TME (C7 cluster), coculturing with C1 cells from *mIDH1* glioma resulted in ~40% inhibition of T cell proliferation ($P < 0.05$), whereas C2 and C3 from *mIDH1* TME did not inhibit T cell proliferation (Fig. 4F). These results validate the inhibitory potential of C1 as the immunosuppressive PMN-MDSCs cluster in *mIDH1* glioma TME.

CD16/32 is a specific marker that defines bona fide immunosuppressive PMN-MDSCs

Our next goal was to identify a specific myeloid marker that would allow us to distinguish the inhibitory PMN-MDSCs from the noninhibitory granulocytes. To identify a unique marker, we used a

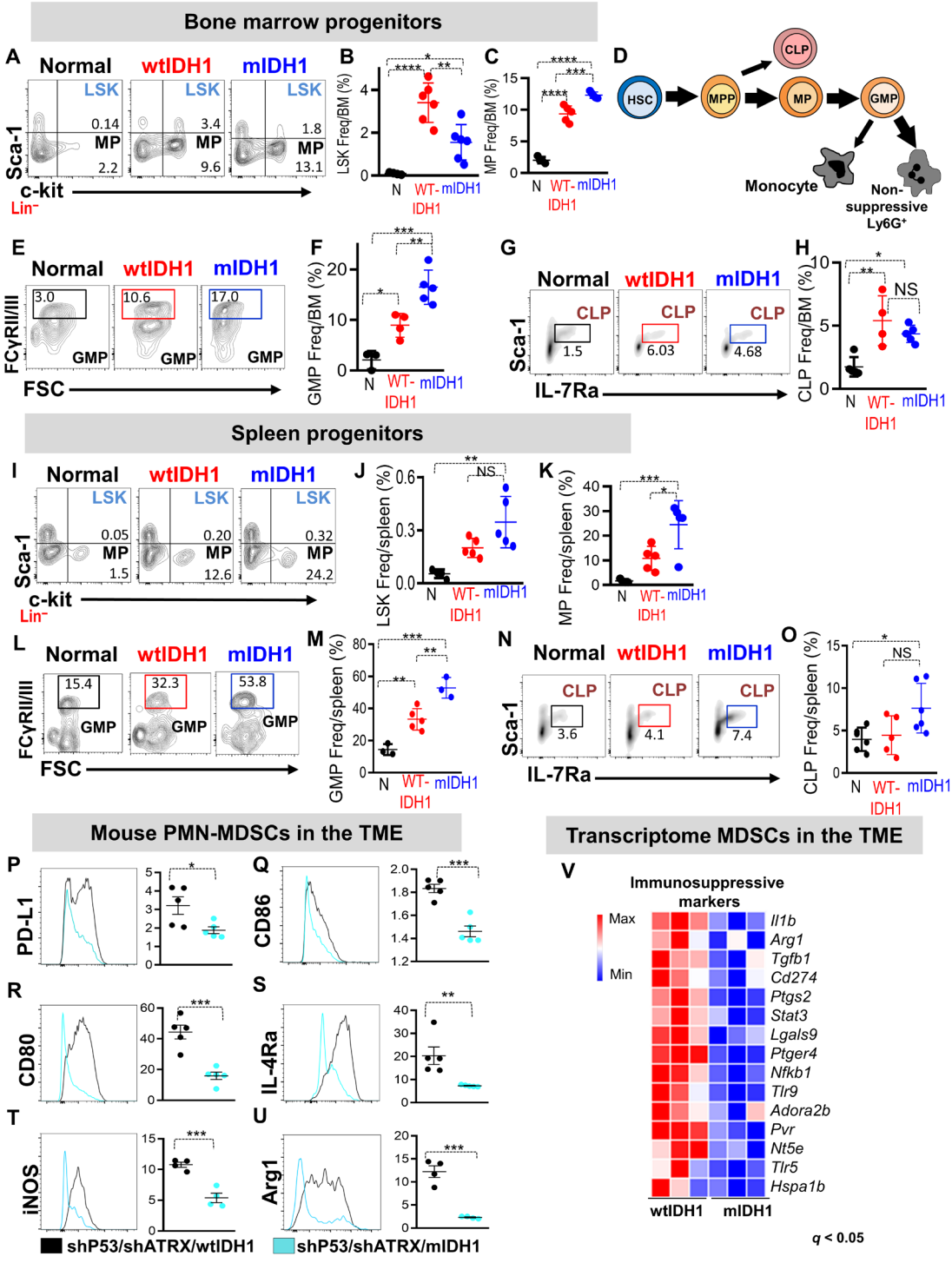

Fig. 3. Phenotypic and molecular characterization of myeloid cell lineages in *mIDH1* glioma. (**A** to **C**) Representative flow cytometry plots and quantification of the percentage of (B) LSK (Lin^-/c-Kit^+/$Sca\text{-}1^+$) and (C) MP (Lin^-/c-Kit^+/$Sca\text{-}1^-$) in BM from normal mice (N), and mice implanted with *wtIDH1* or *mIDH1* neurospheres. (**D**) Schematic diagram representing the shift in myelopoeisis within *mIDH1* tumor–bearing mice. Thick arrows represent predominant developmental pathways in *mIDH1* tumor–bearing mice. (**E** to **H**) Flow cytometry analysis of the frequency of (E and F) GMPs (Lin^-/IL-7Rα^-/c-Kit^+/$Sca\text{-}1^-$/$CD34^+$/FcγRII/III^{high}) and (G and H) CLPs (c-Kit^{low}/$Sca\text{-}1^{low}$/Lin^-/IL-7Rα^+) in the BM from normal and *wtIDH1* or *mIDH1* tumor–bearing mice. (**I** to **K**) Representative flow cytometry plots and quantification of the percentage of (J) LSK and (K) MPs in spleen from normal and *wtIDH1* or *mIDH1* tumor–bearing mice. (**L** and **M**) Representative flow cytometry plot and quantitation analysis showing the frequency of common GMPs in spleens from normal mice and *wtIDH1* and *mIDH1* tumor–bearing animals. (**N** and **O**) Representative flow cytometry plot and quantitation analysis showing the frequency of CLPs in spleens from normal mice, *wtIDH1* and *mIDH1* tumor–bearing mice. (**P** to **U**) Flow cytometry analysis of immunosuppressive/costimulatory markers in the $CD45^{high}$/$CD11b^+$/$Ly6G^+$ population within TME of *wtIDH1* (black) or *mIDH1* (blue). (**V**) Heatmap showing the normalized expression of genes related to PMN-MDSC immunosuppressive signature in myeloid cells ($CD11b^+$/ $Gr\text{-}1^+$) from *wtIDH1* or *mIDH1* TME. *$P < 0.05$, **$P < 0.01$, ***$P < 0.005$, and ****$P < 0.0001$, one-way ANOVA.

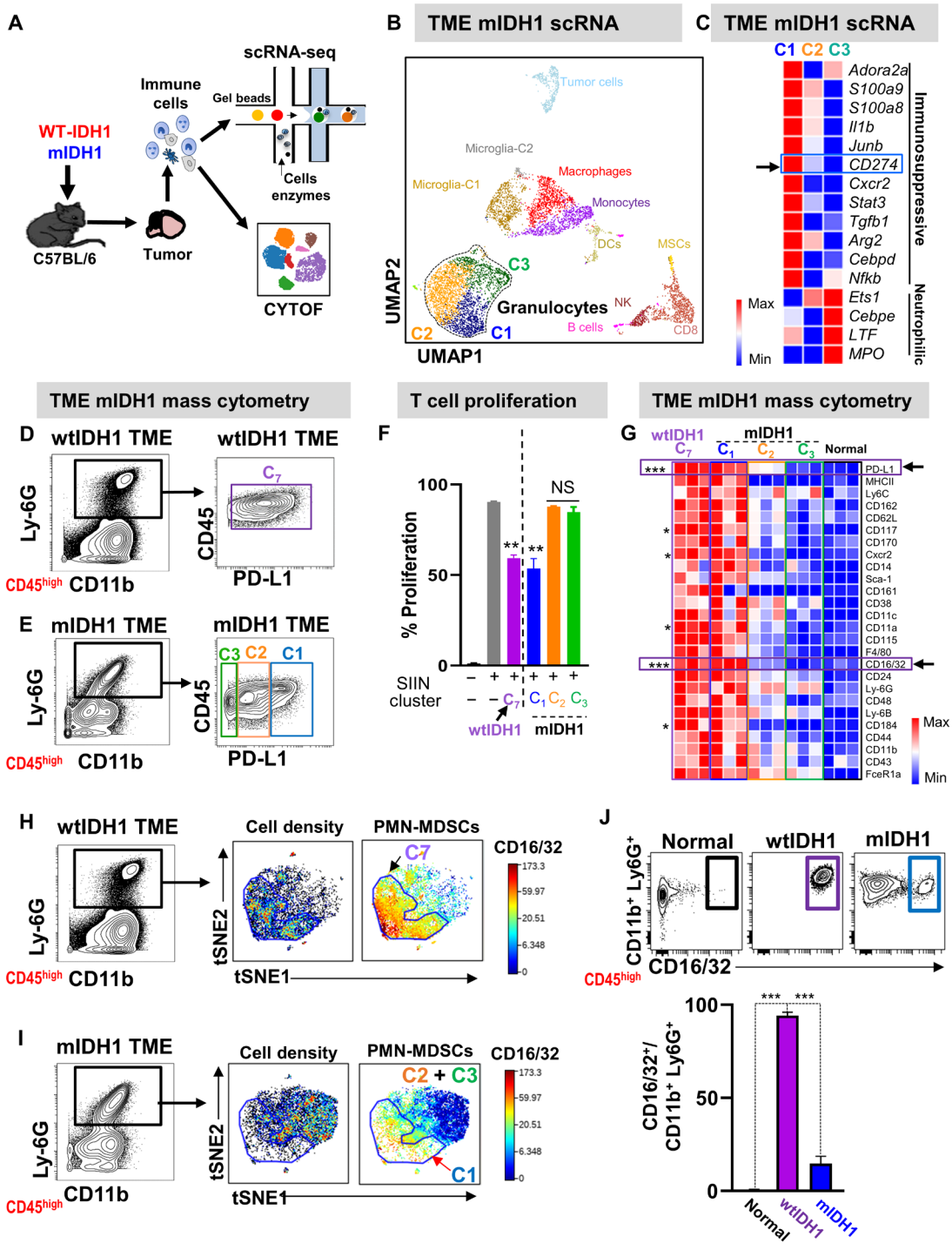

Fig. 4. Nonsuppressive neutrophils and preneutrophils are the major granulocyte population in *mIDH1* tumors. (**A**) Schematic overview of single-cell sequencing and CyTOF analysis of immune cells infiltrating *wtIDH1* and *mIDH1* tumors. (**B**) Combined Seurat analysis of immune cells from *mIDH1* shown in Uniform Manifold Approximation and Projection (UMAP) projection results in various distinct clusters of immune cells ($N = 2$). (**C**) Heatmap of differentially expressed immunosuppressive and neutrophil-related genes between the three granulocytic clusters in *mIDH1* TME. (**D** and **E**) Mass cytometry analysis of granulocytes from TME of (D) *wtIDH1* or (E) *mIDH1* tumors. (**F**) T cell proliferation analysis to assess the inhibitory potential of myeloid cells cluster (C7) from *wtIDH1* tumors and C1, C2, and C3 myeloid cell clusters isolated from *mIDH1* tumors. (**G**) Heatmap representing normalized expression level of myeloid biomarkers within granulocytes from the TME of normal mice, mice implanted with *wtIDH1* tumors, and C1, C2, and C3 clusters from the TME of *mIDH1* tumors. (**H** and **I**) Unsupervised clustering and viSNE visualization of granulocytes from *wtIDH1* (H) or *mIDH1* (I) tumors using the biomarker shown in (G). (**J**) Flow plots and quantitation analysis of the proportion of bona fide PMN-MDSCs ($CD45^{high}/CD11b^{+}/Ly6G^{+}/CD16/32^{+}$) infiltrating normal mice and *wtIDH1* or *mIDH1* tumors. $^{*}P < 0.05$, $^{**}P < 0.01$, $^{***}P < 0.005$, ANOVA.

myeloid-specific antibody panel (table S1) that measures ~30 myeloid-specific parameters simultaneously and used it to perform CyTOF analysis of the granulocytic clusters found in the *mIDH1* and *wtIDH1* glioma TME. We found that granulocytes from *wtIDH1* and the C1 cluster from *mIDH1* TME have similar expression of most of the myeloid biomarkers, with the FC-gamma receptor family (CD16/32) up-regulated in all inhibitory PMN-MDSCs (Fig. 4G). CD16/32 is expressed on macrophages and granulocytes, and its expression is correlated with maturation and function (*32*, *33*). To confirm the correlation between PMN-MDSC phenotype and CD16/32 expression, we performed unsupervised clustering and dimensionality reduction that showed that granulocytes from *mIDH1* TME clustered differently than granulocytes from the *wtIDH1* TME (Fig. 4, H and I). We observed high CD16/32 expression exclusively in all granulocytes from *wtIDH1* and only in C1 from *mIDH1* tumors (Fig. 4, H and I). The majority of granulocytes from *wtIDH1* TME (~95%) express high levels of CD16/32, compared to ~12% of granulocytes in *mIDH1* glioma TME ($P < 0.05$, Fig. 4J). To investigate which gene (CD16 or CD32) is more predominantly expressed by immunosuppressive PMN-MDSCs, we analyzed the difference in expression at the transcriptome level between *Fcgr3* (gene encodes for CD16) and *Fcgr2b* (gene encodes for CD32). Transcriptome analysis showed that *Fcgr3* was the highest in both C7 from *wtIDH1* TME and C1 from *mIDH1* TME (PMN-MDSCs) compared to levels in C2 and C3 *mIDH1* TME (Fig. 5A). In contrast, *Fcgr2b* was not differentially expressed between any cluster (Fig. 5B).

To further validate our finding, we examined the suppressive capacity of tumor-infiltrating $CD45^{high}/CD11b^{+}/Ly6G^{+}/CD16/32^{+}$ or $CD45^{high}/CD11b^{+}/Ly6G^{+}/CD16/32^{-}$ myeloid cells on antigen-specific T cell proliferation. Isolated granulocytes were cocultured with

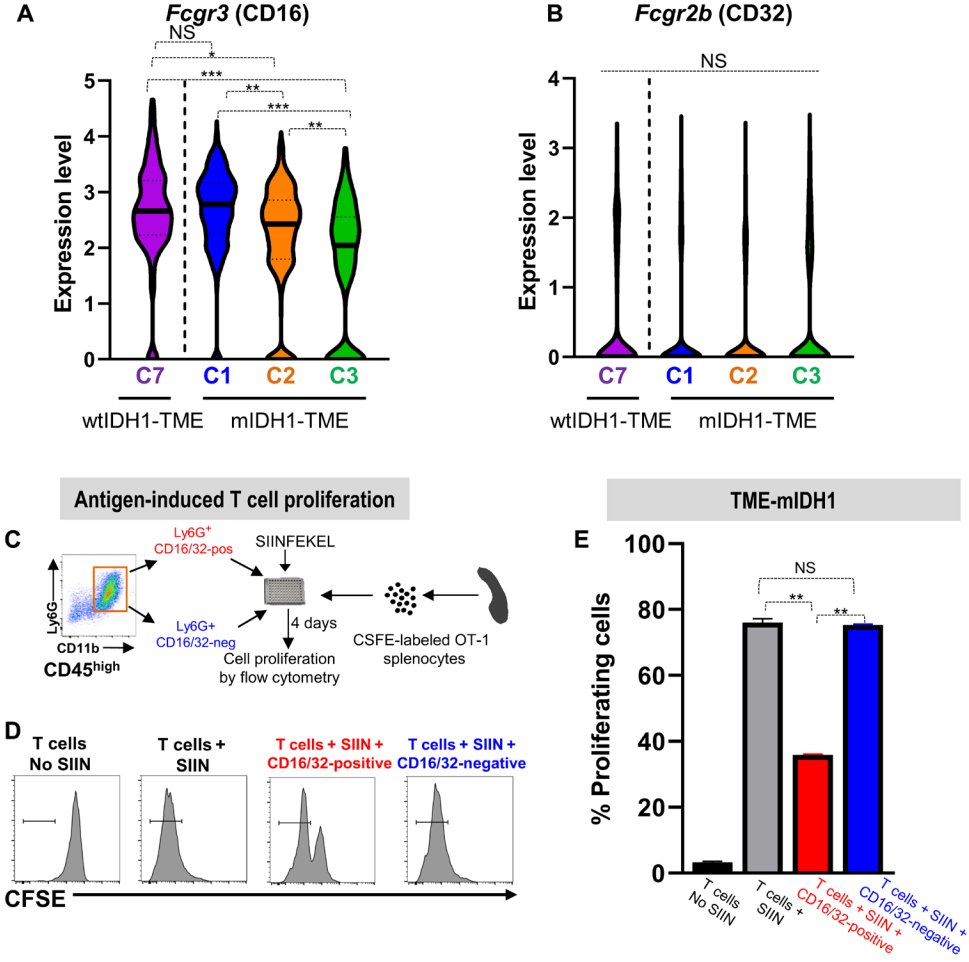

Fig. 5. CD16/32 is a specific marker that defines bona fide immunosuppressive PMN-MDSCs. (**A** and **B**) Violin plot showing the expression of the *Fcgr3* (A) or *Fcgr2b* (B) gene in each granulocytic cluster infiltrating the *wtIDH1* tumor (C7) or *mIDH1* tumors (C1, C2, and C3). *Fcgr3*, but not *Fcgr2b*, is expressed at high level in both immunosuppressive granulocytic MDSCs clusters (C7 and C1). (**C**) Schematic of the in vitro T cell proliferation assay to analyze immune suppressive properties of $CD45^{high}/CD11b^{+}/Ly6G^{+}/CD16/32^{-/+}$. Sorted $CD45^{high}/CD11b^{+}/Ly6G^{+}/CD16/32$-positive or $CD45^{high}/CD11b^{+}/Ly6G^{+}/CD16/32$-negative cells were cocultured with CFSE-labeled splenocytes from *Rag2/OT-1* transgenic mouse. Cultures were stimulated with 100 nM SIINFEKL peptide for 4 days, after which proliferation was analyzed by flow cytometry. (**D**) Representative flow plots showing CFSE staining of unstimulated splenocytes (T only), splenocytes undergoing rapid proliferation in response to SIINFEKL (T + SIIN), and the effect of SIINFEKL-induced T cell proliferation in the presence of $CD45^{high}/CD11b^{+}/Ly6G^{+}/CD16/32$-negative or $CD45^{high}/CD11b^{+}/Ly6G^{+}/CD16/32$-positive cells from the TME of *mIDH1* tumors. (**E**) Quantitation analysis of the inhibitory potential of $CD45^{high}/CD11b^{+}/Ly6G^{+}/CD16/32$-negative or $CD45^{high}/CD11b^{+}/Ly6G^{+}/CD16/32$-positive cells sorted from TME of *mIDH1* tumor. $CD45^{high}/CD11b^{+}/Ly6G^{+}/CD16/32$-positive cells inhibit T cell proliferation, whereas $CD45^{high}/CD11b^{+}/Ly6G^{+}/CD16/32$-negative cells did not suppress T cell proliferation. $^{*}P < 0.05$, $^{**}P < 0.01$, and $^{***}P < 0.005$, one-way ANOVA.

CFSE-labeled splenocytes from OT-1 mice as described before (Fig. 5C). Results showed that only $CD45^{high}/CD11b^{+}/Ly6G^{+}/CD16/32^{+}$ myeloid cells from the TME of *mIDH1* tumors blocked T cell proliferation ~36 ± 3.2% ($P < 0.001$; Fig. 5, D and E). Together, these results establish CD16/32 as a robust and generalizable cell surface marker for immunosuppressive PMN-MDSCs.

PMN-MDSC gene signature is expressed in a higher proportion of tumor-infiltrating immune cells in human *wtIDH1* glioma

We then performed scRNA-seq of immune cells isolated from primary tumor samples of patients with *wtIDH1* and *mIDH1* glioma. We collected 18 patients' glioma samples (8 samples from *wtIDH1* tumors and 10 samples from *mIDH1* tumors). All patients' clinical data are listed in table S5. After performing immune cell purification and applying quality controls, a total of 9765 cells from *wtIDH1* tumors and 17,452 from *mIDH1* tumors were analyzed. *wtIDH1* and *mIDH1* datasets were analyzed separately using Seurat to reproduce cell-type labels (Fig. 6, A and D). Myeloid clusters were the most abundant immune cells infiltrating both the *wtIDH1* and *mIDH1* human gliomas (Fig. 6, A to D). In both groups, there was a total of five clusters of myeloid cells (myeloid C1 to C5) (Fig. 6, A to D); only one cluster (C4) expressed high microglial genes (*C1Qc* and *AIF1*) (Fig. 6, C and D). Similar to the mouse data, the largest cluster in *mIDH1* (myeloid-C1) differentially expressed *CCL3* and *CCL4* (Fig. 6, B and D). Moreover, myeloid-C2 expressed antigen presentation-associated genes (*HLA-A* and *HLA-DRA*), whereas myeloid-C3 expressed granulocyte differentiation genes (*CSF3R* and *NEAT1*; Fig. 6D). We then investigated the expression of the PMN-MDSC gene signature (*IL1β*, *S100a8*, *S100a9*, *ARG1*, and *TGFβ1*) within each cluster in *wtIDH1* and *mIDH1* myeloid cells, separately. The highest PMN-MDSC gene signature was expressed by cells in myeloid-C1 and myeloid-C5 in *wtIDH1* and *mIDH1* tumors, respectively (Fig. 6E). Upon quantification, nearly 23% of all immune cells in *wtIDH1* tumors were PMN-MDSCs, whereas, in the *mIDH1* glioma TME, PMN-MDSCs were only 3.75% of the total immune cells (Fig. 6F). These results are consistent with data from our preclinical model that showed that PMN-MDSCs are present at a higher fraction in the TME of *wtIDH1* glioma than in the TME of *mIDH1* glioma.

G-CSF is the major cytokine that is epigenetically regulated in *mIDH1* glioma

Our data demonstrate that most of the granulocytes found in *mIDH1* TME are noninhibitory granulocytes. We hypothesized that the change in granulocytes' phenotype and function is due to epigenetic reprogramming, which affects cytokine expression in the *mIDH1* glioma cells. Therefore, we profiled cytokines known to influence myeloid differentiation in conditioned media collected from *wtIDH1* or *mIDH1* cultured mouse glioma neurospheres. GM-CSF, CXCL1, CXCL10, IL-5, macrophage inflammatory protein 2, IL-6, and tumor necrosis factor–α were among the downregulated cytokines in *mIDH1* conditioned media (Fig. 7A and fig. S15). However, G-CSF, Regulated on activation, normal T cell expressed and secreted (RANTES) (CCL5), IL-33, and Stem Cell Factor (SCF) were the only cytokines that were up-regulated in *mIDH1*-conditioned media (fig. S15). To investigate whether these cytokines were epigenetically regulated by *mIDH1*, we used a chromatin immunoprecipitation sequencing (ChIP-seq) dataset that we have recently reported [National Center for Biotechnology Information (NCBI) Omnibus identifier: GSE99806], which was obtained using SB-generated neurospheres with *mIDH1* and *wtIDH1* (*19*). Gene promoters enriched for H3K4me3 peaks are generally associated with transcriptional activation. Among the genes encoding the cytokines that were up-regulated in conditioned media from *mIDH1*, only *Csf3* showed a marked change in the peak enrichment for H3K4me3 mark around the promoter region (Fig. 7, B and C). To uncover the epigenetic mechanisms of *CSF3* regulation in *mIDH1* glioma, we performed ChIP-seq analysis on SF10602 (patient-derived glioma cells expressing *mIDH1*, inactivating mutations in *ATRX* and *TP53*) after treatment with vehicle or 5 μM of the *mIDH1* inhibitor (AG1-5198) for 7 days (Fig. 7D). At the *CSF3* locus, we observed a down-regulation of H3K4me3 deposition upstream of the transcriptional start site at the gene promoter region in SF10602 treated with *mIDH1* inhibitor (AGI-5198, blue) compared to untreated SF10602 (gray) (Fig.7, E to I). There was no significant deposition of H3K6me3, H3K27ac, and H3K27me3 in both groups (Fig. 7, F, G, and I). Moreover, there was no difference in the H3K4me1 deposition around the *CSF3* promoter region between SF10602 treated with vehicle versus AGI-5198 (Fig. 7H). These results suggest that *mIDH1* is responsible for the epigenetic regulation of the *CSF3* expression.

To demonstrate the increase in G-CSF in *mIDH1* glioma, we performed quantitative enzyme-linked immunosorbent assay (ELISA) in the mouse serum of tumor-bearing animals, as well as in conditioned media from cultured mouse and human neurospheres. In all cases, the level of G-CSF was increased in *mIDH1* compared to *wtIDH1* (~5-fold, $P < 0.05$; Fig. 7, J to L). Of note, the levels of G-CSF in the conditioned media were not altered when *mIDH1* neurospheres were cultured in FBS-containing media (fig. S16). In addition, transcriptome analysis of patients with astrocytoma in TCGA revealed that *CSF3* gene expression was significantly up-regulated in patients with *mIDH1* glioma harboring *ATRX* and *TP53* mutations (Fig. 7M). The increased level of G-CSF in *mIDH1* could explain the significant expansion of granulocytes in *mIDH1* tumor–bearing mice as well as the enrichment of the cytokine signaling pathway triggered by G-CSF receptor expressed on myeloid cells. To further validate the enhanced G-CSF secretion in *mIDH1* glioma, we collected serum samples from 16 glioma patients with *wtIDH1* or *mIDH1* glioma and analyzed the G-CSF levels by quantitative ELISA. All patients' clinical information is shown in table S5. Of note, none of the patients had any prior treatments with Temozolomide (TMZ) or commercially available rG-CSF. Results showed that the G-CSF level was higher in patients with glioma with *mIDH1* compared to those with *wtIDH1* (Fig. 7N).

Glioma *mIDH1* stem/progenitor-like cells are the major source of G-CSF expression

To uncover the source of G-CSF within *mIDH1* tumors, we performed scRNA-seq of whole tumors (~6000 cells) isolated from the SB-induced *mIDH1* glioma model. Results show that most of the *Csf3* were expressed by the major tumor cell clusters, which belong to stem-like cells (Fig. 8, A to C). These cells express genes such as *Tcf4, Sox9*, *Sox11*, and *Sox4* (Fig. 8, D to G). This suggests that the undifferentiated glioma cells from *mIDH1* tumors express high levels of G-CSF, resulting in the phenotypic remodeling of the granulocytic myeloid cells.

G-CSF is a growth factor that promotes the survival and differentiation of early MP cells into neutrophils by binding to its

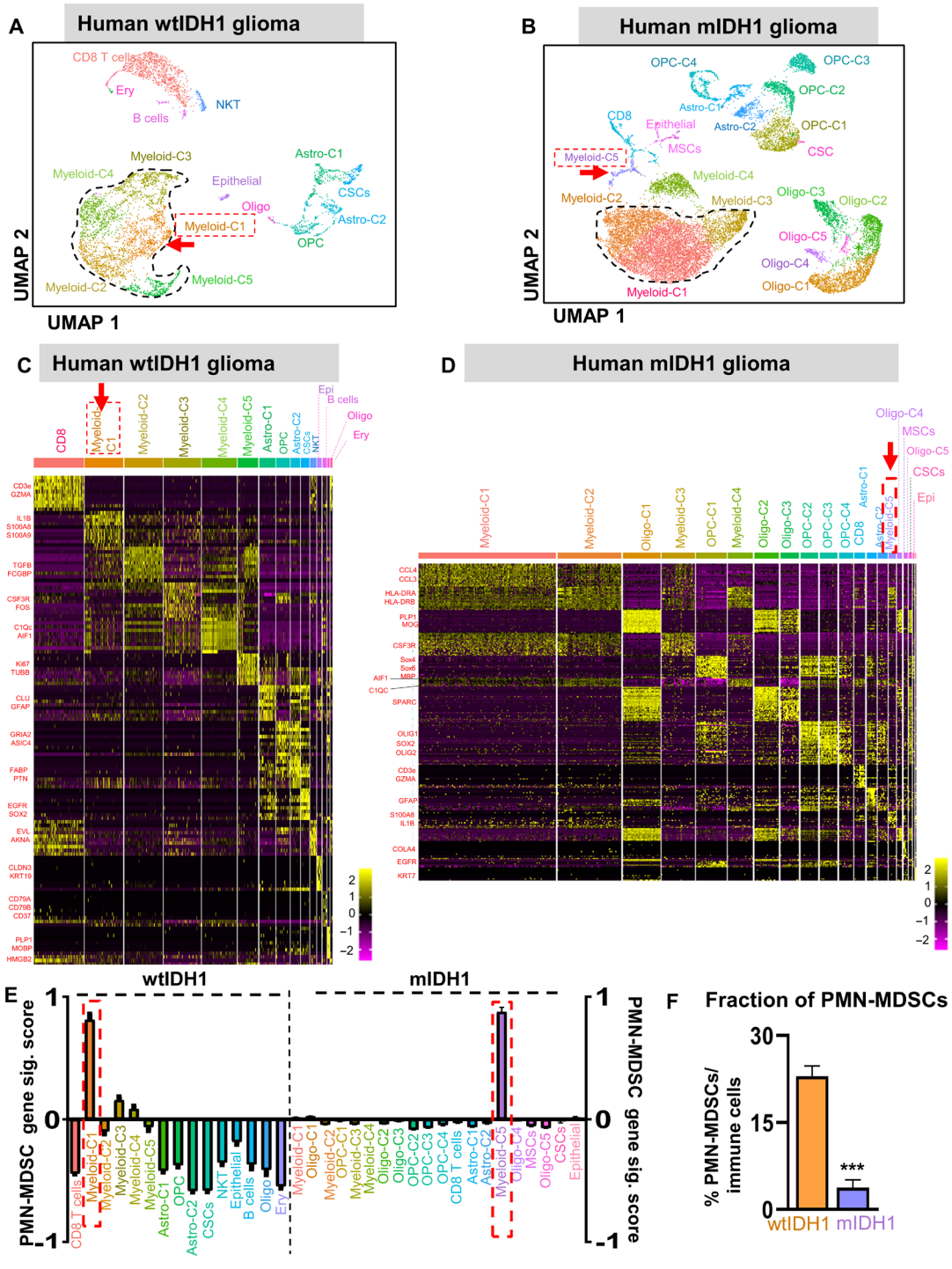

Fig. 6. PMN-MDSC gene signature is expressed in a higher proportion of tumor-infiltrating immune cells in human *wtIDH1* glioma. Seurat analysis of immune cells from (**A**) *wtIDH1* or (**B**) *mIDH1* primary tumor samples, shown in UMAP projection, results in various distinct clusters. (**C** and **D**) Heatmaps showing the differentially expressed genes in each cluster of (C) *wtIDH1* tumor and (D) *mIDH1* tumor samples. (**E**) Bar plots showing the relative PMN-MDSC gene signature score in each cluster of primary human samples. (**F**) Quantification of the tumor-infiltrating PMN-MDSCs/total immune cells calculated from scRNA-seq data. ***$P < 0.001$, Student's *t* test.

primary receptor GCSFR. To examine the GCSFR expression on glioma cells, we analyzed its expression by flow cytometry using multiple patient-derived glioma cell cultures including SJ-GBM2-*wtIDH1*, SJ-GBM2-*mIDH1*, MGG8-*wtIDH1*, MGG8-*mIDH1*, LC1035-*mIDH1*, and SF10602-*mIDH1* cells. Data showed that all human-derived cell cultures do not express GCSFR (Fig. 8, H to N). Similarly, cultured mouse neurospheres do not express GCSFR, whereas the majority of GCSFR expression was on myeloid cells ($CD11b^+$ $Gr\text{-}1^+$) within the TME of both *wtIDH1* and *mIDH1* glioma–bearing mice (Fig. 8, O to S).

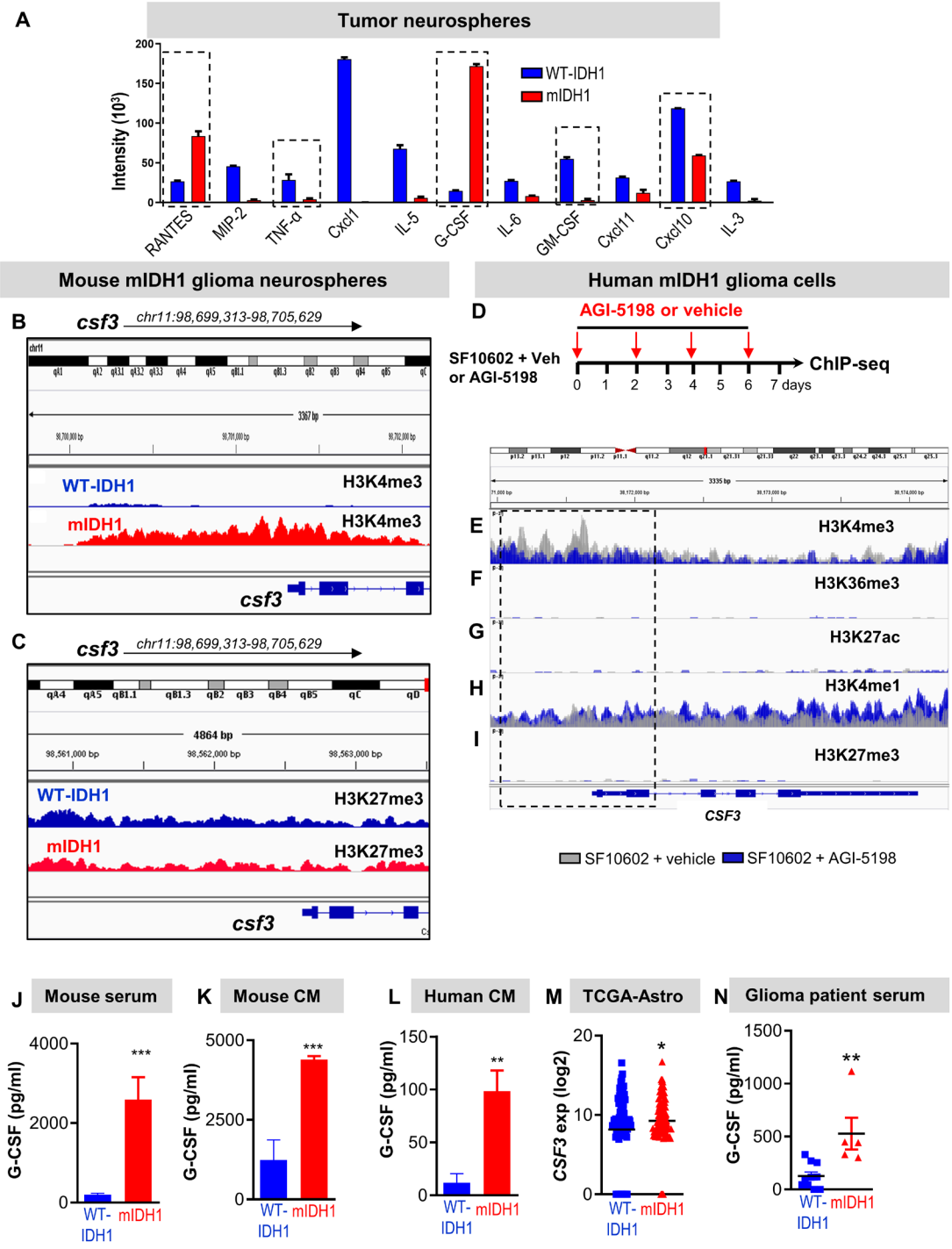

Fig. 7. G-CSF is a major epigenetically regulated cytokine expressed by glioma stem-like cells. (**A**) Cytokine array analysis performed on conditioned media from *wtIDH1* and *mIDH1* neurospheres. (**B**) H3K4me3 and (**C**) H3K27me3 occupancy at specific genomic regions of *Csf3* gene. (**D**) Experimental design for ChIP-seq analysis of mIDH1 patient-derived neurospheres (SF10602) treated with vehicle or the *mIDH1* inhibitor (AGI-5198). (**E** to **I**) Histone marks occupancy at specific genomic regions of *CSF3* gene in SF10602 treated with *mIDH1* inhibitor (AGI-5198, blue) compared to untreated cells (gray). (**J** to **L**) Quantitative ELISA of the G-CSF level in mouse serum of tumor-bearing animals (J), conditioned media from cultured mouse neurospheres (K), and conditioned media from cultured human neurospheres (L) expressing *wtIDH1* or *mIDH1*. (**M**) Analysis of TCGA data for *CSF3* gene expression in *mIDH1* glioma patients harboring *TP53* and *ATRX* mutation ($n = 99$) and *wtIDH1* ($n = 82$). (**N**) Quantitative ELISA of serum G-CSF from glioma patients with *wtIDH1* or *mIDH1* (astrocytoma). $^*P < 0.05$, $^{**}P < 0.01$, and $^{***}P < 0.005$, Student's *t* test.

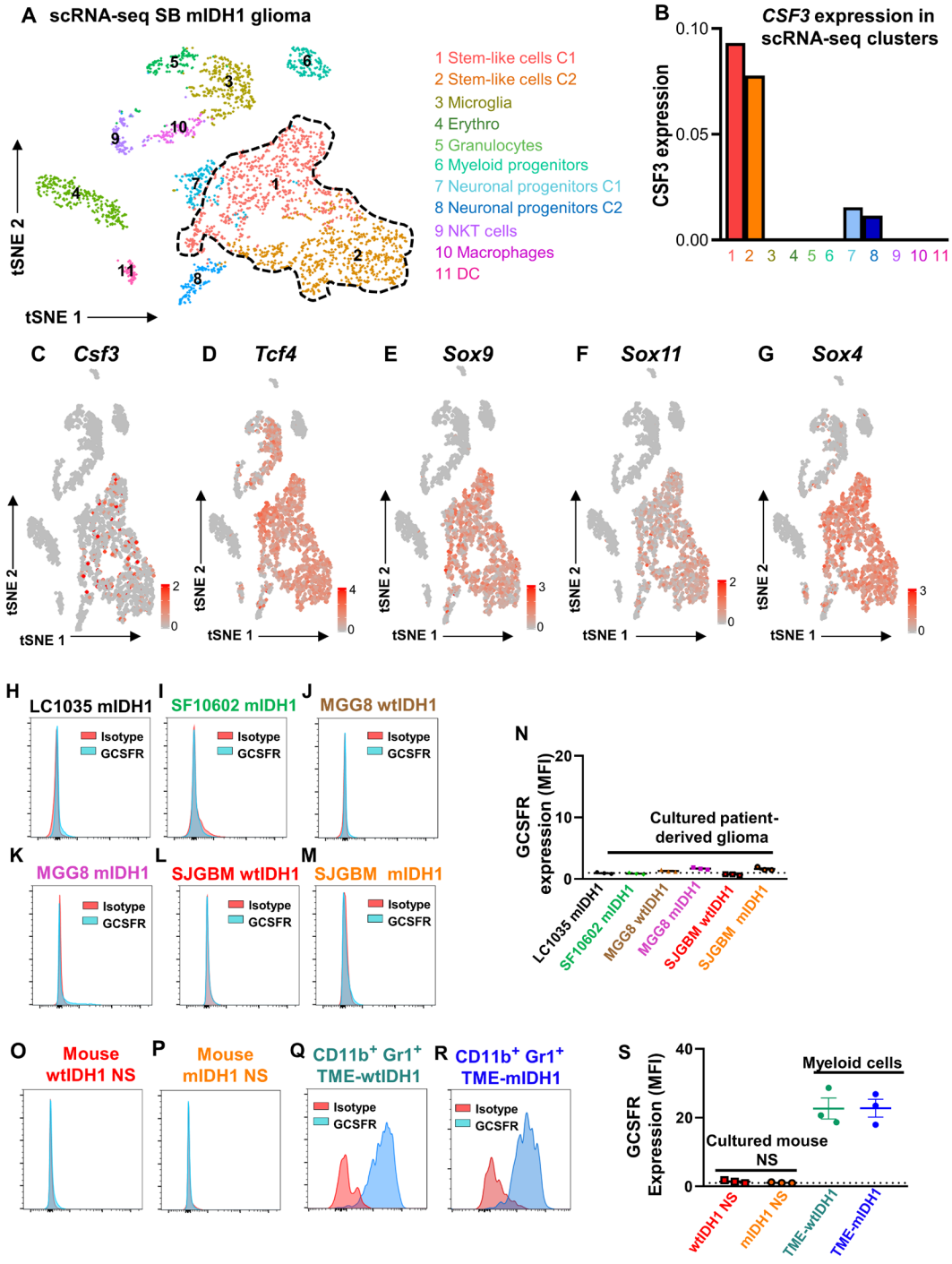

Fig. 8. Glioma *mIDH1* stem-like cells are the major source of G-CSF expression. (**A** and **B**) Combined Seurat analysis shown in tSNE projection of whole tumor from *mIDH1* GEMM of glioma resulted in various distinct clusters of cells. The expression of *CSF3* was analyzed between the clusters. Stem-like cells were the major clusters that have the highest *CSF3* expression ($N = 2$). (**C** to **G**) Feature plots represent the expression of (C) *csf3*, (D) *tcf4*, (E) *sox9*, (F) *sox11*, and (G) *sox4*. (**H** to **M**) Flow cytometry analysis of the GCSFR expression in glioma patient-derived cells with *wtIDH1* or *mIDH1*. (**N**) Quantification of GCSFR expression in cultured human glioma cells with *wtIDH1* or *mIDH1*. MFI, Mean fluorescence intensity. (**O** and **P**) Flow cytometry analysis of the GCSFR expression in mouse neurospheres developed by the SB model with *wtIDH1* or *mIDH1*. (**Q** and **R**) Flow cytometry analysis of the GCSFR expression on $CD11b^+$ $Gr\text{-}1^+$ derived from the TME of *wtIDH1* or *mIDH1* tumor–bearing mice. (**S**) Quantification of GCSFR expression in conditions (O) to (R).

G-CSF neutralization restores the immunosuppressive properties of CD45^{high}/CD11b^{+}/Ly6G^{+} in *mIDH1* TME

If the CD45^{high}/CD11b^{+}/Ly6G^{+} phenotype in *mIDH1* is dependent on G-CSF expression, blocking G-CSF should reverse their immune-permissive phenotype. We depleted G-CSF in the *mIDH1* tumor–bearing animals using αG-CSF neutralizing antibody (Fig. 9A). Treatment with αG-CSF significantly reduced the serum levels of G-CSF in *mIDH1* tumor–bearing mice (~86 and ~92% decrease in day 14 dpi and 21 dpi, respectively; Fig. 9B, $P < 0.01$) and decreased the frequency of granulocytes in the TME, spleen, and BM (~40, ~63, and ~10%, respectively, $P < 0.05$; Fig. 9C). G-CSF neutralization remodeled the CD45^{high}/CD11b^{+}/Ly6G^{+} compartment within the TME of *mIDH1* tumor–bearing animals to an inhibitory phenotype, which resulted in ~35% inhibition of T cell proliferation (Fig. 9D). Moreover, G-CSF neutralization shortened the MS of *mIDH1* (but not the *wtIDH1*) tumor–bearing animals ($P < 0.05$; Fig. 9E). This demonstrates that the noninhibitory properties of granulocytes in the *mIDH1* glioma–bearing mice are driven by high secretion of G-CSF by glioma cells.

CSF3 expression is associated with a favorable outcome only in patients with glioma harboring *mIDH1*

Tumor-derived G-CSF has been shown to promote tumor progression and enhance metastasis in several tumor types (*34*, *35*). To evaluate the effect of G-CSF in patients with glioma, we turned to the TCGA data and analyzed the MS of all tumor types available in the context of G-CSF (*CSF3*) expression (i.e., MS of patients expressing high versus low levels of *CSF3*). Out of 24 tumor types in the TCGA portal, we found that lower-grade glioma with *mIDH1* was the only tumor type in which a significant difference existed between the MS of patients with high versus low *CSF3* expression (Fig. 9, H to M, and fig. S17). Moreover, when we stratified the patients with astrocytoma according to *mIDH1* and *CSF3* expression, we found that enhanced MS related to high *CSF3* expression was solely observed in patients with *mIDH1* glioma tumors (Fig. 9F). We validated these results using the Chinese Glioma Genome Atlas in which we found that in secondary Glioblastoma (GBM), patients with *mIDH1* tumors expressing high *CSF3* level have a better prognosis compared to patients with low *CSF3* (Fig. 9G). In both datasets, there were no significant differences in MS between high versus low expression of other cytokines responsible for PMN-MDSC development such as *CSF1*, *IL4*, *IL1β*, *TNFα*, and *IL6* in patients with *mIDH1* (fig S18). These results suggest a unique correlation between G-CSF expression in patients with *mIDH1* glioma and patient prognosis.

Glioma-derived G-CSF induces the expansion of neutrophils and enhances the efficacy of TK/Flt3L immunotherapy

To uncover whether G-CSF alone is sufficient to induce the expansion of nonimmunosuppressive neutrophils, we dosed *wtIDH1* tumor–bearing mice with recombinant G-CSF (Fig. 10A). We used rG-CSF (2 μg/day) to achieve steady-state serum G-CSF concentrations comparable to levels observed in *mIDH1* tumor–bearing mice (Fig. 10A) and similar to reported doses (*36*). Compared to vehicle-treated animals, *wtIDH1* tumor–bearing animals treated with rG-CSF showed expansion of CD45^{high}/CD11b^{+}/Ly6G^{+} cells in the TME (Fig. 10B). These granulocytes expressed lower levels of CD16/32 and PD-L1 compared to granulocytes from vehicle-treated control and did not inhibit T cell proliferation (Fig. 10, C to E). rG-CSF administration significantly prolonged the MS of tumor-bearing animals in two different *wtIDH1* glioma models (Fig. 10, F and G). These results supported the hypothesis that G-CSF leads to the expansion of nonimmune suppressive neutrophils, validated the association between increased G-CSF secretion, and enhanced prognosis in glioma. To address the exact effects of G-CSF on other immune cells within the *wtIDH1* TME, we performed high-dimensional immune profiling using CyTOF analysis of the tumor-infiltrating immune cells from *wtIDH1* tumor–bearing animals treated with either rG-CSF or vehicle as described in Fig. 10A (fig. S19A). Results showed that rG-CSF treatment results in a significant increase in CD45^{high}/CD11b^{+}/Ly6G^{+} cells in the TME ($P < 0.005$; fig. S19B). Beside the decrease in macrophages in the rG-CSF group ($P < 0.05$; fig. S19C), there was no significant difference in other immune cells tested (fig. S19, D to I). To validate the source of G-CSF, *wtIDH1* neurospheres were stably transduced with lentivirus encoding G-CSF (lenti–G-CSF) or with an empty lentivirus vector (lenti-vector). Successfully transduced neurospheres were cultured in vitro for 14 days before they were used for implantation (fig. S20A). The enhanced G-CSF expression was confirmed by reverse transcription quantitative polymerase chain reaction (RT-qPCR) and by ELISA in conditioned media of cultured neurospheres (fig. S20, B and C). As expected, results showed that animals implanted with *wtIDH1*–lenti–G-CSF neurospheres had increased CD45^{high}/CD11b^{+}/Ly6G^{+} cells within the tumor, spleen, and BM compared to mice implanted with *wtIDH1*–lenti-vector neurospheres (fig. S20, D to F). Collectively, these data demonstrate the effect of tumor-derived G-CSF on the phenotype and function of granulocytes in *mIDH1* glioma.

Since rG-CSF results in expansion of nonimmunosuppressive granulocytes, we asked whether rG-CSF would synergize with the TK/Flt3L gene therapy and prolong mice survival in a high-grade glioma model with *wtIDH1*. Neurospheres with *wtIDH1* were implanted in mice, rG-CSF was administered in a daily dose for 14 consecutive days, and TK/Flt3L was given on day 7 after implantation (Fig. 10H). TK/Flt3L enhanced the MS of *wtIDH1* tumor–bearing mice, but combination therapy (TK/Flt3L + rG-CSF) further prolonged the MS of mice with *wtIDH1* tumor ($P < 0.05$, Fig. 10I). These results suggest that rG-CSF further enhanced the efficacy of TK/Flt3L gene therapy.

The data presented here elucidate new potential therapeutic approaches that can enhance antiglioma immunotherapy. A model figure of the proposed molecular mechanism by which *mIDH1* remodels tumor-infiltrating granulocytes to noninhibitory neutrophils is shown in Fig. 10J. Through epigenetic reprogramming caused by the presence of 2HG, *mIDH1* stem-like cells express a high level of G-CSF that shifts the hematopoiesis in BM and spleen toward the expansion, differentiation, and mobilization of granulocytic myeloid cells. The granulocytes recruited to the TME in *mIDH1* tumors are mainly neutrophils and preneutrophils, with a small fraction of PMN-MDSCs. Overall, the expanded granulocytes in *mIDH1* TME do not suppress T cell function and enhanced the efficacy of immunotherapy.

DISCUSSION

Advances in genomics and epigenomics revealed the molecular and epigenetic identity of *mIDH1* glioma, which is elicited mainly by 2HG-mediated inhibition of the methylcytosine dioxygenase TET2 and αKG-dependent histone demethylases. The resulting

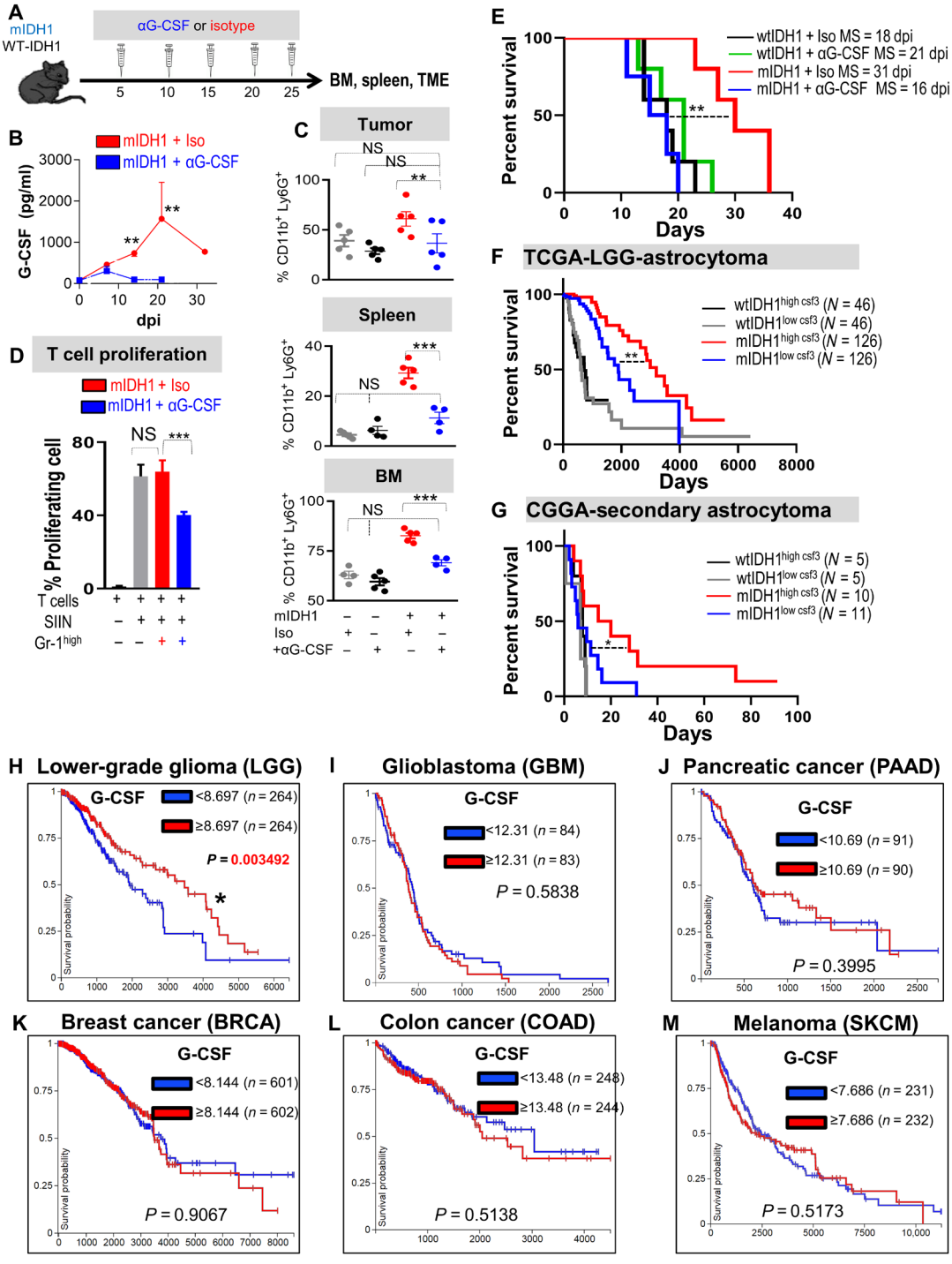

Fig. 9. G-CSF neutralization restores the immunosuppressive properties in myeloid cells and enhances the efficacy of immunotherapy. (**A**) Schematic showing experimental design of G-CSF neutralization in *wtIDH1* and *mIDH1* tumor–bearing mice. (**B**) Quantitative ELISA of serum G-CSF from *mIDH1* glioma-bearing mice treated with either isotype (red) or αG-CSF (blue). (**C**) Flow analysis of $CD45^{high}/CD11b^{+}/Ly6G^{+}$ cells from tumor, spleen, and BM of tumor-bearing mice treated with either isotype or αG-CSF. (**D**) T cell proliferation assay of $CD45^{high}/CD11b^{+}/Ly6G^{+}$ infiltrating *mIDH1* tumor treated with isotype or αG-CSF. (**E**) Kaplan-Meier survival analysis of mice implanted with either *wtIDH1* or *mIDH1* neurospheres treated with isotype or αG-CSF. (**F**) Kaplan-Meier survival analysis of TCGA-LGG astrocytoma *wtIDH1* or *mIDH1* patients with high and low *CSF3* expression. (**G**) Kaplan-Meier survival analysis of Chinese Glioma Genome Atlas (CGGA)–secondary astrocytoma *wtIDH1* or *mIDH1* patients with high and low levels of *CSF3* expression. (**H** to **M**) Kaplan-Meier survival analysis of the different types of tumors in the TCGA data according to *CSF3* expression (high or low). LGG is the sole tumor within the TCGA database in which patients who express a high level of *CSF3* have a favorable prognosis compared to patients with low *CSF3* expression. **P* < 0.05, ***P* < 0.01, and ****P* < 0.005, ANOVA.

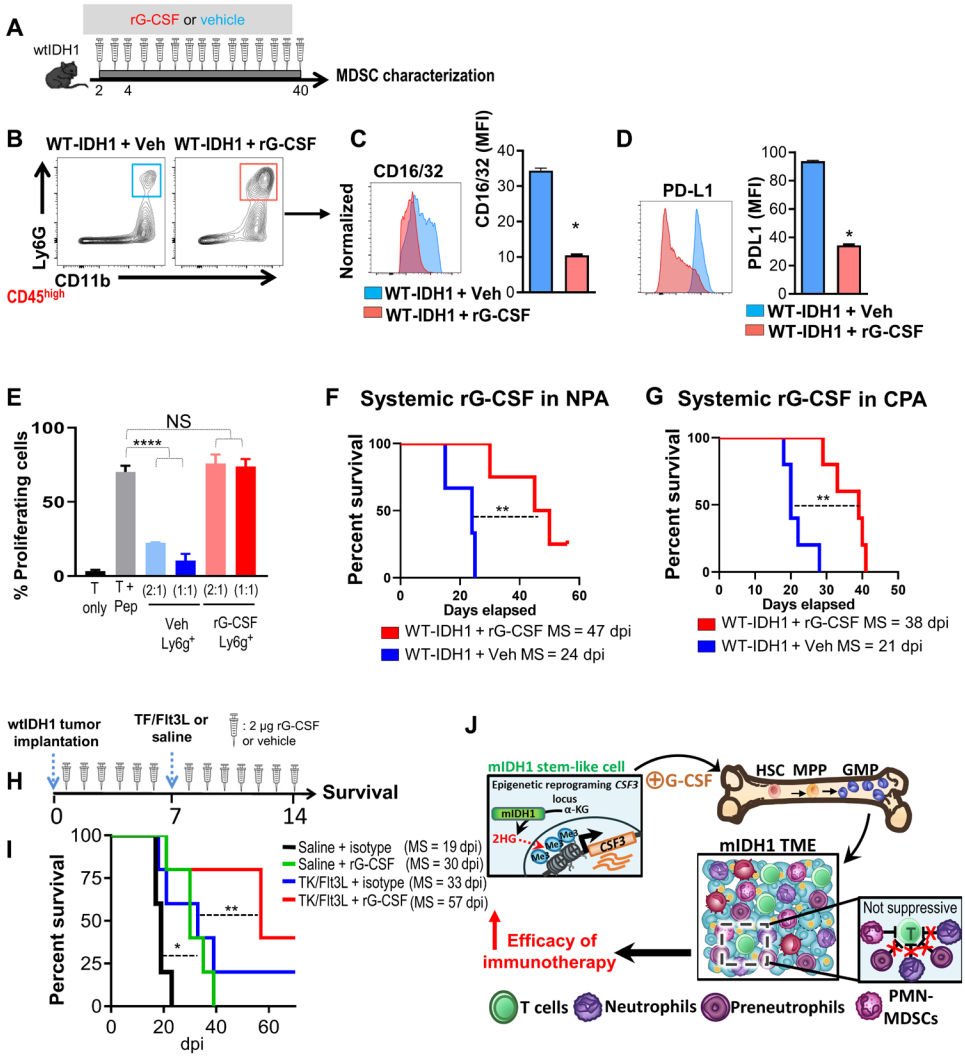

Fig. 10. G-CSF induces the expansion of nonsuppressive neutrophils and enhances the efficacy of TK/Flt3L immunotherapy in *wtIDH1* glioma. (**A**) Experimental design of rG-CSF or vehicle administration in *wtIDH1* tumor–bearing animals. (**B**) Flow analysis of granulocytes infiltrating *wtIDH1* tumors after treatment with vehicle or rG-CSF. (**C** and **D**) Flow analysis of CD16/32 and PD-L1 expression on granulocytes isolated from *wtIDH1* tumor–bearing animals treated with vehicle (blue) or rG-CSF (red). (**E**) Flow analysis of the inhibitory potential of $CD45^{high}/CD11b^{+}/Ly6G^{+}$ cells isolated from TME of *wtIDH1* tumor–bearing mice treated with vehicle (blue) or with rG-CSF (red). (**F** and **G**) Kaplan-Meier survival analysis of mice bearing *wtIDH1* tumors (F) (NPA) or (G) (CPA) treated with either isotype (blue) or rG-CSF (red). (**H**) Schematic diagram illustrates the treatment strategy of the TK + Flt3L gene therapy in combination with rG-CSF in *wtIDH1* tumor–bearing mice. (**I**) Kaplan-Meier survival curves of mice bearing *wtIDH1* tumors, treated with TK + Flt3L, rG-CSF, or combination therapy. (**J**) Proposed model of aberrant granulocyte differentiation in the *mIDH1* tumor. $^{*}P < 0.05$, $^{**}P < 0.01$, and $^{****}P < 0.0001$, ANOVA.

genome-wide hypermethylation phenotype influences both glioma development and the TME (*37*).

Gliomas are characterized by a profound immunosuppressive milieu that is responsible, at least in part, for hindering the efficacy of immunotherapies in clinical settings (*14*, *38*). Previous studies have shown that patients with glioblastoma have elevated levels of circulating MDSCs, the majority of which (~82%) belong to PMN-MDSCs and are associated with poor prognosis (*17*, *39*, *40*). We have recently shown that the PMN-MDSCs are the predominant immunosuppressive myeloid cells that, upon depletion, significantly enhanced the efficacy of immunotherapy and prolonged MS in *wtIDH1* glioma–bearing mice (*12*). Our data illustrated that myeloid cells infiltrating the *mIDH1* glioma, counter to these infiltrating the *wtIDH1* gliomas, express low levels of immunosuppressive genes and did not inhibit T cell function. This explains the significant differences in the efficacy of immunotherapy (TK/Flt3L) between *wtIDH1* and *mIDH1* glioma–bearing mice. In line with these results, myeloid depletion further enhances the efficacy of TK/Flt3L in the *wtIDH1*, but not in the *mIDH1* gliomas, highlighting the immune permissive microenvironment in *mIDH1* glioma.

Gliomas are highly heterogeneous tumors, having both intertumor and intratumor heterogeneity at the cellular and genomic levels (*41*–*43*). The mechanism by which genetic heterogeneity influences the tumor immune microenvironment remains elusive (*44*, *45*). The use of scRNA-seq technologies has now provided additional granularity that enables charting of subtypes of immune cellular infiltrates within the glioma microenvironment. This technology enabled us to identify the developmental hierarchies within the

glioma-infiltrating myelopoietic cell clusters, uncovering novel drivers and revealing the infiltrating-immune surveillance/evasion cell types relevant to glioma with specific genetic lesions (*43*, *46*, *47*). Transcriptome profiling at the single-cell level uncovered the heterogeneity of infiltrating myeloid lineages. We found that the *mIDH1* glioma–infiltrating granulocytes are composed of three distinct cell clusters: C1, C2, and C3. Differential gene expression analysis between the three clusters identified that cluster C1 was enriched in immunosuppressive PMN-MDSC signature marker genes such as *Tgfb*, *Il1b*, and *Arg2*. Cluster C2 expressed *S100a8*, *Ccl3*, *Ccl4*, and cell cycle genes such as *Cdc20* and *G0s2*, indicating proliferating neutrophils (preneutrophils), whereas C3 expressed neutrophil maturation genes such as *Cebpe* and *Mpo*. In contrast, in the *wtIDH1* glioma model, the tumor-infiltrating granulocytes are composed of single-cluster expressing genes similar to granulocyte cluster C1 in the *mIDH1* group.

Since a hallmark of MDSCs is their inhibition of antigen-specific $CD8^+$ T cell proliferation, we next aimed to isolate the three newly identified granulocytic clusters encountered within the *mIDH1* TME for functional characterization. An ideal marker would be expressed on the cell surface and have different expression levels between the three clusters. Interrogation of the differentially expressed genes between C1, C2, and C3 revealed that *CD274* (PD-L1) was expressed at a high level in PMN-MDSCs (cluster C1) compared to intermediate and low levels in the preneutrophils (cluster C2) and neutrophils (cluster C3), respectively. This allowed us to isolate each cluster and examine their T cell inhibitory potential. Using this approach, we found that in the *mIDH1* group, cells in cluster C1 were suppressive, whereas the cells in cluster C2 and C3 were nonimmunosuppressive. In the *wtIDH1* group, granulocytes expressing PD-L1 formed one single-cell cluster (C7), which inhibited $CD8^+$ T cell proliferation. Last, we performed in-depth high-dimensional mass cytometry characterization and phenotypic analysis of the three granulocytic clusters found in the *mIDH1* TME. An advantage of this approach is that automated clustering is done on data reduced to two tSNE dimensions, which allows visual verification of cluster boundaries at the single-cell resolution. Combined clustering of granulocytes infiltrating the TME of *mIDH1* or *wtIDH1* GEMMs of glioma revealed that most of the granulocytes from the *wtIDH1* tumor coclustered with the C1 cluster of the *mIDH1* group. CyTOF analysis also led to the identification of CD16/32 as a unique and reproducible myeloid marker that can be used to distinguish immunosuppressive PMN-MDSCs from nonimmunosuppressive granulocytes.

Consistent with results from our GEMMs of glioma, we found that most of the immune cells infiltrating human gliomas expressing *mIDH1* exhibit characteristic myeloid cells' gene signatures, all of which express the early granulocytic receptor GCSFR. The largest myeloid cluster in the human *mIDH1* glioma group expressed genes (*CCL3* and *CCL4*) similar to cluster C2 in our *mIDH1* GEMM of glioma. Moreover, using a unique PMN-MDSC gene signature, our data elucidated that human *mIDH1* gliomas exhibit a lower frequency of tumor-infiltrating bona fide PMN-MDSCs when compared to the patients with *wtIDH1* glioma. Therefore, the molecular and phenotypic features of *mIDH1* on tumor-infiltrating PMN-MDSCs are largely conserved between our mouse model and human samples.

We also show that G-CSF was up-regulated in the conditioned media of cultured human and mouse *mIDH1* NS. This increase was also significant in the serum from patients with *mIDH1* astrocytoma and *mIDH1* tumor–bearing mice. We demonstrated that the increased G-CSF expression in *mIDH1* neurospheres was due to epigenetic reprogramming of the tumor cells' transcriptome, in which the *CSF3* gene showed an enrichment in the deposition of the H3K4me3 mark around the promoter region. We demonstrated that in our *mIDH1* GEMM of glioma, tumor cells express a higher level of *Sox2* and are less differentiated (*19*); this is consistent with earlier reports indicating that $IDH1^{R132H}$ suppresses cellular differentiation (*4*, *48*). scRNA-seq revealed that glioma stem-like cells that express *Sox2* and *Sox4* are the major source of G-CSF expression in *mIDH1* tumors. Therefore, the enhanced production of G-CSF is due to the presence of a higher proportion of less-differentiated tumor cells in *mIDH1* glioma. In line with this, studies showed that within the glioma niche, glioma stem-like cells are found to be coenriched with myeloid-infiltrating immune cells (*49*).

The impact of G-CSF on tumor biology is still a point of debate. rG-CSF (Filgastim) is a commercially available product indicated for chemo-induced neutropenia to reverse myelosuppression in patients with cancer, and it has been shown to reduce inflammation and reverse cognitive impairment in patients with Alzheimer (*50*, *51*). In addition, increased G-CSF secretion has been implicated in the recruitment and infiltration of immunosuppressive MDSCs in breast cancer (*34*) and cervical cancer (*35*). In contrast, in mice bearing MCA203 sarcomas, G-CSF induced $CD11b^+/Gr\text{-}1^{hi}$ cells that were nonsuppressive (*52*). It has also been shown that the administration of G-CSF leads to the formation of nonimmunosuppressive $CD45^+/CD11b^+/Gr\text{-}1^+$ cells in vivo (*52*) and in vitro (*53*). Our data in *mIDH1* glioma show that the increased production of G-CSF by *mIDH1* glioma stem-like cells caused the expansion of $CD45^{high}/CD11b^+/Ly6G^+$ cells that exhibit a nonimmunosuppressive phenotype. We also showed that rG-CSF administration to mice harboring *wtIDH1* glioma expands nonsuppressive myeloid cells, leading to enhanced efficacy of immunostimulatory gene therapy TK/Flt3L in glioma mice with *wtIDH1*. In summary, our data demonstrate that *mIDH1* tumor–derived G-CSF reprograms myelopoiesis in glioma, which promotes the production of nonimmunosuppressive myeloid cells, a feature that can be harnessed to enhance immunotherapeutic efficacy in patients with *mIDH1* LGG.

MATERIALS AND METHODS

Human subjects

All patients gave informed consent for collection of clinical correlates, tissue collection, and research testing under Institutional Review Board–approved protocols (HUM00057130, UMCC 2015.024). Patient clinical information is listed in table S5. Patient studies were conducted according to the Declaration of Helsinki, the Belmont Report, and the U.S. Common Rule.

Experimental model and subject details

Six- to 8-week-old wild-type C57BL/6 female mice (Taconic) were housed under standard specific pathogen–free conditions. All animal procedures were carried out in accordance with the University of Michigan's Institutional Animal Care and Use Committee. All animals were housed in an American Association for Accreditation of Laboratory Animal Care (AAALAC)–accredited animal facility.

Study design

To study the impact of glioma $IDH1^{R123H}$ on myeloid cell phenotype and function, we generated a genetically engineered animal

model injecting SB plasmids encoding NRA G12V, *shATRX*, and *shp53* with or without $IDH1^{R132H}$ (*wtIDH1* and *mIDH1*, respectively) into the lateral ventricle of neonatal mice (*19*–*21*). Sample size and any data inclusion/exclusion were defined individually for each experiment. We also used an animal model generated by intracranial implantation of glioma NS (*wtIDH1* and *mIDH1*) derived from our genetically engineered animal model (*19*). In addition, we used two alternative animal models that do not encode RAS-activating mutations [(*PDGFB/shP53/shATRX/Ink4a/Arf*$^{-/-}$ *wtIDH1*-NS or *mIDH1*-NS) and (*CDKN2A*$^{-/-}$*/shP53/shATRX/wtIDH1*-NS or *mIDH1*-NS)]. We performed pan characterization of all immune cells by flow cytometry and mass cytometry and identified each immune cell population using unique biomarkers. Detailed information regarding the source of antibodies and immune cells' gating are listed in tables S1, S2, and S3. We also performed scRNA-seq to define the PMN-MDSC cell population in both mouse and human glioma tissue derived from patients harboring $IDH1^{R132H}$ or *wtIDH1*. We validated PMN-MDSCs by functional analysis of T cell's inhibitory characteristics. All sequencing datasets have been deposited in NCBI's Gene Expression Omnibus with identifier (GSE152277). CyTOF data are deposited in Immport (accession number: SDY1774). Materials and Methods related to tumor implantation, RNA-seq, T cell proliferation assay, ChIP-seq, cytokine analysis, RT-qPCR, and scRNA-seq are described in detail in the Supplementary Materials.

Statistical analysis

Sample sizes were selected on the basis of preliminary data from pilot experiments and previously published results in the literature and our laboratory. Unpaired Student's *t* test or one-way analysis of variance (ANOVA), followed by Tukey's multiple comparisons posttest, was utilized for comparing experimental groups with controls from flow cytometry analysis, cytokine analysis, mass cytometry analysis, and T cell functional assays. RNA-seq data were processed using the Tuxedo Suite, and differentially expressed genes were considered when false discovery rate ≤ 0.05 and fold change $\geq \pm 1.5$. All single-cell sequencing data were processed by Cell Ranger Pipeline version 3.1.0. Filtered digital gene expression matrix file matrices containing the number of unique molecular identifier counts per gene per cell were analyzed using the Seurat R package version 3.1.4. Statistically significant principal components were determined using the jackstraw function (*28*, *31*). All quantitative data are presented as the means ± SEM from at least three independent samples. ANOVA and two-sample *t* tests were used to compare continuous outcomes between groups. Survival curves were analyzed using the Kaplan-Meier method and compared using Mantel-Cox tests; the effect size is expressed as MS. Differences were considered significant if $P < 0.05$. All analyses were conducted using GraphPad Prism software (version 8.00) or R (version 3.4). The statistical tests used are indicated in each figure legend.

SUPPLEMENTARY MATERIALS

Supplementary material for this article is available at https://science.org/doi/10.1126/sciadv.abh3243

View/request a protocol for this paper from *Bio-protocol*.

REFERENCES AND NOTES

1. M. Ceccarelli, F. P. Barthel, T. M. Malta, T. S. Sabedot, S. R. Salama, B. A. Murray, O. Morozova, Y. Newton, A. Radenbaugh, S. M. Pagnotta, S. Anjum, J. Wang, G. Manyam, P. Zoppoli, S. Ling, A. A. Rao, M. Grifford, A. D. Cherniack, H. Zhang, L. Poisson, C. G. Carlotti Jr., D. P. C. Tirapelli, A. Rao, T. Mikkelsen, C. C. Lau, W. K. A. Yung, R. Rabadan, J. Huse, D. J. Brat, N. L. Lehman, J. S. Barnholtz-Sloan, S. Zheng, K. Hess, G. Rao, M. Meyerson, R. Beroukhim, L. Cooper, R. Akbani, M. Wrensch, D. Haussler, K. D. Aldape, P. W. Laird, D. H. Gutmann, H. Noushmehr, A. Iavarone, R. G. W. Verhaak, S. Anjum, H. Arachchi, J. T. Auman, M. Balasundaram, S. Balu, G. Barnett, S. Baylin, S. Bell, C. Benz, N. Bir, K. L. Black, T. Bodenheimer, L. Boice, M. S. Bootwalla, J. Bowen, C. A. Bristow, Y. S. N. Butterfield, Q. R. Chen, L. Chin, J. Cho, E. Chuah, S. Chudamani, S. G. Coetzee, M. L. Cohen, H. Colman, M. Couce, F. D'Angelo, T. Davidsen, A. Davis, J. A. Demchok, K. Devine, L. Ding, R. Duell, J. B. Elder, J. M. Eschbacher, A. Fehrenbach, M. Ferguson, S. Frazer, G. Fuller, J. Fulop, S. B. Gabriel, L. Garofano, J. M. Gastier-Foster, N. Gehlenborg, M. Gerken, G. Getz, C. Giannini, W. J. Gibson, A. Hadjipanayis, D. N. Hayes, D. I. Heiman, B. Hermes, J. Hilty, K. A. Hoadley, A. P. Hoyle, M. Huang, S. R. Jefferys, C. D. Jones, S. J. M. Jones, Z. Ju, A. Kastl, A. Kendler, J. Kim, R. Kucherlapati, P. H. Lai, M. S. Lawrence, S. Lee, K. M. Leraas, T. M. Lichtenberg, P. Lin, Y. Liu, J. Liu, J. Y. Ljubimova, Y. Lu, Y. Ma, D. T. Maglinte, H. S. Mahadeshwar, M. A. Marra, M. McGraw, C. McPherson, S. Meng, P. A. Mieczkowski, C. R. Miller, G. B. Mills, R. A. Moore, L. E. Mose, A. J. Mungall, R. Naresh, T. Naska, L. Neder, M. S. Noble, A. Noss, B. P. O'Neill, Q. T. Ostrom, C. Palmer, A. Pantazi, M. Parfenov, P. J. Park, J. S. Parker, C. M. Perou, C. R. Pierson, T. Pihl, A. Protopopov, A. Radenbaugh, N. C. Ramirez, W. K. Rathmell, X. Ren, J. Roach, A. G. Robertson, G. Saksena, J. E. Schein, S. E. Schumacher, J. Seidman, K. Senecal, S. Seth, H. Shen, Y. Shi, J. Shih, K. Shimmel, H. Sicotte, S. Sifri, T. Silva, J. V. Simons, R. Singh, T. Skelly, A. E. Sloan, H. J. Sofia, M. G. Soloway, X. Song, C. Sougnez, C. Souza, S. M. Staugaitis, H. Sun, C. Sun, D. Tan, J. Tang, Y. Tang, L. Thorne, F. A. Trevisan, T. Triche, D. J. van den Berg, U. Veluvolu, D. Voet, Y. Wan, Z. Wang, R. Warnick, J. N. Weinstein, D. J. Weisenberger, M. D. Wilkerson, F. Williams, L. Wise, Y. Wolinsky, J. Wu, A. W. Xu, L. Yang, L. Yang, T. I. Zack, J. C. Zenklusen, J. Zhang, W. Zhang, J. Zhang, E. Zmuda, Molecular profiling reveals biologically discrete subsets and pathways of progression in diffuse glioma. *Cell* **164**, 550–563 (2016).
2. H. Yan, D. W. Parsons, G. Jin, R. McLendon, B. A. Rasheed, W. Yuan, I. Kos, I. Batinic-Haberle, S. Jones, G. J. Riggins, H. Friedman, A. Friedman, D. Reardon, J. Herndon, K. W. Kinzler, V. E. Velculescu, B. Vogelstein, D. D. Bigner, IDH1 and IDH2 mutations in gliomas. *N. Engl. J. Med.* **360**, 765–773 (2009).
3. M. E. Figueroa, O. Abdel-Wahab, C. Lu, P. S. Ward, J. Patel, A. Shih, Y. Li, N. Bhagwat, A. Vasanthakumar, H. F. Fernandez, M. S. Tallman, Z. Sun, K. Wolniak, J. K. Peeters, W. Liu, S. E. Choe, V. R. Fantin, E. Paietta, B. Löwenberg, J. D. Licht, L. A. Godley, R. Delwel, P. J. M. Valk, C. B. Thompson, R. L. Levine, A. Melnick, Leukemic IDH1 and IDH2 mutations result in a hypermethylation phenotype, disrupt TET2 function, and impair hematopoietic differentiation. *Cancer Cell* **18**, 553–567 (2010).
4. C. Lu, P. S. Ward, G. S. Kapoor, D. Rohle, S. Turcan, O. Abdel-Wahab, C. R. Edwards, R. Khanin, M. E. Figueroa, A. Melnick, K. E. Wellen, D. M. O'Rourke, S. L. Berger, T. A. Chan, R. L. Levine, I. K. Mellinghoff, C. B. Thompson, IDH mutation impairs histone demethylation and results in a block to cell differentiation. *Nature* **483**, 474–478 (2012).
5. P. S. Ward, J. Patel, D. R. Wise, O. Abdel-Wahab, B. D. Bennett, H. A. Coller, J. R. Cross, V. R. Fantin, C. V. Hedvat, A. E. Perl, J. D. Rabinowitz, M. Carroll, S. M. Su, K. A. Sharp, R. L. Levine, C. B. Thompson, The common feature of leukemia-associated IDH1 and IDH2 mutations is a neomorphic enzyme activity converting alpha-ketoglutarate to 2-hydroxyglutarate. *Cancer Cell* **17**, 225–234 (2010).
6. N. M. Amankulor, Y. Kim, S. Arora, J. Kargl, F. Szulzewsky, M. Hanke, D. H. Margineantu, A. Rao, H. Bolouri, J. Delrow, D. Hockenbery, A. M. G. Houghton, E. C. Holland, Mutant IDH1 regulates the tumor-associated immune system in gliomas. *Genes Dev.* **31**, 774–786 (2017).
7. L. Mu, Y. Long, C. Yang, L. Jin, H. Tao, H. Ge, Y. E. Chang, A. Karachi, P. S. Kubilis, G. de Leon, J. Qi, E. J. Sayour, D. A. Mitchell, Z. Lin, J. Huang, The IDH1 mutation-induced oncometabolite, 2-hydroxyglutarate, may affect DNA methylation and expression of PD-L1 in Gliomas. *Front. Mol. Neurosci.* **11**, 82 (2018).
8. A. S. Berghoff, B. Kiesel, G. Widhalm, D. Wilhelm, O. Rajky, S. Kurscheid, P. Kresl, A. Wöhrer, C. Marosi, M. E. Hegi, M. Preusser, Correlation of immune phenotype with IDH mutation in diffuse glioma. *Neuro Oncol.* **19**, 1460–1468 (2017).
9. P. J. Cimino, M. Zager, L. McFerrin, H. G. Wirsching, H. Bolouri, B. Hentschel, A. von Deimling, D. Jones, G. Reifenberger, M. Weller, E. C. Holland, Multidimensional scaling of diffuse gliomas: Application to the 2016 World Health Organization classification system with prognostically relevant molecular subtype discovery. *Acta Neuropathol. Commun.* **5**, 39–39 (2017).
10. P. Kadiyala, S. V. Carney, J. C. Gauss, M. B. Garcia-Fabiani, S. Haase, M. S. Alghamri, F. J. Núñez, Y. Liu, M. Yu, A. Taher, F. M. Nunez, D. Li, M. B. Edwards, C. G. Kleer, H. Appelman, Y. Sun, L. Zhao, J. J. Moon, A. Schwendeman, P. R. Lowenstein, M. G. Castro, Inhibition of 2-hydroxyglutarate elicits metabolic reprogramming and mutant IDH1 glioma immunity in mice. *J. Clin. Invest.* **131**, e139542 (2021).
11. Z. Chen, X. Feng, C. J. Herting, V. A. Garcia, K. Nie, W. W. Pong, R. Rasmussen, B. Dwivedi, S. Seby, S. A. Wolf, D. H. Gutmann, D. Hambardzumyan, Cellular and molecular identity of tumor-associated macrophages in glioblastoma. *Cancer Res.* **77**, 2266–2278 (2017).
12. N. Kamran, P. Kadiyala, M. Saxena, M. Candolfi, Y. Li, M. A. Moreno-Ayala, N. Raja, D. Shah, P. R. Lowenstein, M. G. Castro, Immunosuppressive myeloid cells' blockade in the glioma

microenvironment enhances the efficacy of immune-stimulatory gene therapy. *Mol. Ther.* **25**, 232–248 (2017).
13. D. N. Louis, A. Perry, G. Reifenberger, A. von Deimling, D. Figarella-Branger, W. K. Cavenee, H. Ohgaki, O. D. Wiestler, P. Kleihues, D. W. Ellison, The 2016 World Health Organization classification of tumors of the central nervous system: A summary. *Acta Neuropathol.* **131**, 803–820 (2016).
14. N. Kamran, M. S. Alghamri, F. J. Nunez, D. Shah, A. S. Asad, M. Candolfi, D. Altshuler, P. R. Lowenstein, M. G. Castro, Current state and future prospects of immunotherapy for glioma. *Immunotherapy* **10**, 317–339 (2018).
15. A. L. Chang, J. Miska, D. A. Wainwright, M. Dey, C. V. Rivetta, D. Yu, D. Kanojia, K. C. Pituch, J. Qiao, P. Pytel, Y. Han, M. Wu, L. Zhang, C. M. Horbinski, A. U. Ahmed, M. S. Lesniak, CCL2 produced by the glioma microenvironment is essential for the recruitment of regulatory T cells and myeloid-derived suppressor cells. *Cancer Res.* **76**, 5671–5682 (2016).
16. B. Raychaudhuri, P. Rayman, P. Huang, M. Grabowski, D. Hambardzumyan, J. H. Finke, M. A. Vogelbaum, Myeloid derived suppressor cell infiltration of murine and human gliomas is associated with reduction of tumor infiltrating lymphocytes. *J. Neurooncol* **122**, 293–301 (2015).
17. D. Dubinski, J. Wölfer, M. Hasselblatt, T. Schneider-Hohendorf, U. Bogdahn, W. Stummer, H. Wiendl, O. M. Grauer, $CD4^+$ T effector memory cell dysfunction is associated with the accumulation of granulocytic myeloid-derived suppressor cells in glioblastoma patients. *Neuro Oncol.* **18**, 807–818 (2015).
18. P. R. Gielen, B. M. Schulte, E. D. Kers-Rebel, K. Verrijp, H. M. J. M. Petersen-Baltussen, M. ter Laan, P. Wesseling, G. J. Adema, Increase in both CD14-positive and CD15-positive myeloid-derived suppressor cell subpopulations in the blood of patients with glioma but predominance of CD15-positive myeloid-derived suppressor cells in glioma tissue. *J. Neuropathol. Exp. Neurol.* **74**, 390–400 (2015).
19. F. J. Nunez, F. M. Mendez, P. Kadiyala, M. S. Alghamri, M. G. Savelieff, M. B. Garcia-Fabiani, S. Haase, C. Koschmann, A.-A. Calinescu, N. Kamran, M. Saxena, R. Patel, S. Carney, M. Z. Guo, M. Edwards, M. Ljungman, T. Qin, M. A. Sartor, R. Tagett, S. Venneti, J. Brosnan-Cashman, A. Meeker, V. Gorbunova, L. Zhao, D. M. Kremer, L. Zhang, C. A. Lyssiotis, L. Jones, C. J. Herting, J. L. Ross, D. Hambardzumyan, S. Hervey-Jumper, M. E. Figueroa, P. R. Lowenstein, M. G. Castro, IDH1-R132H acts as a tumor suppressor in glioma via epigenetic up-regulation of the DNA damage response. *Sci. Transl. Med.* **11**, eaaq1427 (2019).
20. C. Koschmann, A.-A. Calinescu, F. J. Nunez, A. Mackay, J. Fazal-Salom, D. Thomas, F. Mendez, N. Kamran, M. Dzaman, L. Mulpuri, J. Krasinkiewicz, R. Doherty, R. Lemons, J. A. Brosnan-Cashman, Y. Li, S. Roh, L. Zhao, H. Appelman, D. Ferguson, V. Gorbunova, A. Meeker, C. Jones, P. R. Lowenstein, M. G. Castro, ATRX loss promotes tumor growth and impairs nonhomologous end joining DNA repair in glioma. *Sci. Transl. Med.* **8**, 328ra328 (2016).
21. A.-A. Calinescu, F. J. Núñez, C. Koschmann, B. L. Kolb, P. R. Lowenstein, M. G. Castro, Transposon mediated integration of plasmid DNA into the subventricular zone of neonatal mice to generate novel models of glioblastoma. *J. Vis. Exp* **2015**, 52443 (2015).
22. S. Ali, G. D. King, J. F. Curtin, M. Candolfi, W. Xiong, C. Liu, M. Puntel, Q. Cheng, J. Prieto, A. Ribas, J. Kupiec-Weglinski, N. van Rooijen, H. Lassmann, P. R. Lowenstein, M. G. Castro, Combined immunostimulation and conditional cytotoxic gene therapy provide long-term survival in a large glioma model. *Cancer Res.* **65**, 7194–7204 (2005).
23. A. K. Ghulam Muhammad, M. Candolfi, G. D. King, K. Yagiz, D. Foulad, Y. Mineharu, K. M. Kroeger, K. A. Treuer, W. S. Nichols, N. S. Sanderson, J. Yang, M. Khayznikov, N. Van Rooijen, P. R. Lowenstein, M. G. Castro, Antiglioma immunological memory in response to conditional cytotoxic/immune-stimulatory gene therapy: Humoral and cellular immunity lead to tumor regression. *Clin. Cancer Res.* **15**, 6113–6127 (2009).
24. S. C. Bendall, E. F. Simonds, P. Qiu, E. D. Amir, P. O. Krutzik, R. Finck, R. V. Bruggner, R. Melamed, A. Trejo, O. I. Ornatsky, R. S. Balderas, S. K. Plevritis, K. Sachs, D. Pe'er, S. D. Tanner, G. P. Nolan, Single-cell mass cytometry of differential immune and drug responses across a human hematopoietic continuum. *Science* **332**, 687–696 (2011).
25. A. D. Amirel, K. L. Davis, M. D. Tadmor, E. F. Simonds, J. H. Levine, S. C. Bendall, D. K. Shenfeld, S. Krishnaswamy, G. P. Nolan, D. Pe'er, viSNE enables visualization of high dimensional single-cell data and reveals phenotypic heterogeneity of leukemia. *Nat. Biotechnol.* **31**, 545–552 (2013).
26. R. V. Bruggner, B. Bodenmiller, D. L. Dill, R. J. Tibshirani, G. P. Nolan, Automated identification of stratifying signatures in cellular subpopulations. *Proc. Natl. Acad. Sci.* **111**, E2770–E2777 (2014).
27. D. Hambardzumyan, N. M. Amankulor, K. Y. Helmy, O. J. Becher, E. C. Holland, Modeling adult gliomas using RCAS/t-va technology. *Transl. Oncol.* **2**, 89–95 (2009).
28. A. Butler, P. Hoffman, P. Smibert, E. Papalexi, R. Satija, Integrating single-cell transcriptomic data across different conditions, technologies, and species. *Nat. Biotechnol.* **36**, 411–420 (2018).
29. H. Alshetaiwi, N. Pervolarakis, L. L. M. Intyre, D. Ma, Q. Nguyen, J. A. Rath, K. Nee, G. Hernandez, K. Evans, L. Torosian, A. Silva, C. Walsh, K. Kessenbrock, Defining the emergence of myeloid-derived suppressor cells in breast cancer using single-cell transcriptomics. *Sci. Immunol.* **5**, eaay6017 (2020).
30. K. Honey, CCL3 and CCL4 actively recruit $CD8^+$ T cells. *Nat. Rev. Immunol.* **6**, 427–427 (2006).
31. T. Stuart, A. Butler, P. Hoffman, C. Hafemeister, E. Papalexi, W. M. Mauck III, Y. Hao, M. Stoeckius, P. Smibert, R. Satija, Comprehensive integration of single-cell data. *Cell* **177**, 1888–1902.e21 (2019).
32. M. T. Elghetany, Surface antigen changes during normal neutrophilic development: A critical review. *Blood Cell. Mol. Dis.* **28**, 260–274 (2002).
33. C. Lambert, F. W. M. B. Preijers, G. Yanikkaya Demirel, U. Sack, Monocytes and macrophages in flow: An ESCCA initiative on advanced analyses of monocyte lineage using flow cytometry. *Cytometry B Clin. Cytom.* **92**, 180–188 (2017).
34. A. J. Casbon, D. Reynaud, C. Park, E. Khuc, D. D. Gan, K. Schepers, E. Passegué, Z. Werb, Invasive breast cancer reprograms early myeloid differentiation in the bone marrow to generate immunosuppressive neutrophils. *Proc. Natl. Acad. Sci. U.S.A.* **112**, E566–E575 (2015).
35. M. Kawano, S. Mabuchi, Y. Matsumoto, T. Sasano, R. Takahashi, H. Kuroda, K. Kozasa, K. Hashimoto, A. Isobe, K. Sawada, T. Hamasaki, E. Morii, T. Kimura, The significance of G-CSF expression and myeloid-derived suppressor cells in the chemoresistance of uterine cervical cancer. *Sci. Rep.* **5**, 18217 (2015).
36. M. A. Meyer, J. M. Baer, B. L. Knolhoff, T. M. Nywening, R. Z. Panni, X. Su, K. N. Weilbaecher, W. G. Hawkins, C. Ma, R. C. Fields, D. C. Linehan, G. A. Challen, R. Faccio, R. L. Aft, D. G. DeNardo, Breast and pancreatic cancer interrupt IRF8-dependent dendritic cell development to overcome immune surveillance. *Nat. Commun.* **9**, 1250 (2018).
37. D. W. Parsons, S. Jones, X. Zhang, J. C.-H. Lin, R. J. Leary, P. Angenendt, P. Mankoo, H. Carter, I. M. Siu, G. L. Gallia, A. Olivi, R. M. Lendon, B. A. Rasheed, S. Keir, T. Nikolskaya, Y. Nikolsky, D. A. Busam, H. Tekleab, L. A. Diaz Jr., J. Hartigan, D. R. Smith, R. L. Strausberg, S. K. N. Marie, S. M. O. Shinjo, H. Yan, G. J. Riggins, D. D. Bigner, R. Karchin, N. Papadopoulos, G. Parmigiani, B. Vogelstein, V. E. Velculescu, K. W. Kinzler, An integrated genomic analysis of human glioblastoma multiforme. *Science* **321**, 1807–1812 (2008).
38. M. B. Garcia-Fabiani, M. Ventosa, A. Comba, M. Candolfi, A. J. N. Candia, M. S. Alghamri, P. Kadiyala, S. Carney, S. M. Faisal, A. Schwendeman, J. J. Moon, L. Scheetz, J. Lahann, A. Mauser, P. R. Lowenstein, M. G. Castro, Immunotherapy for gliomas: Shedding light on progress in preclinical and clinical development. *Expert Opin. Investig. Drugs* **29**, 659–684 (2020).
39. B. Raychaudhuri, P. Rayman, J. Ireland, J. Ko, B. Rini, E. C. Borden, J. Garcia, M. A. Vogelbaum, J. Finke, Myeloid-derived suppressor cell accumulation and function in patients with newly diagnosed glioblastoma. *Neuro Oncol.* **13**, 591–599 (2011).
40. Y. Gan, X. Zhou, X. Niu, J. Li, T. Wang, H. Zhang, Y. Yang, Y. Liu, Q. Mao, Neutrophil/lymphocyte ratio is an independent prognostic factor in elderly patients with high-grade gliomas. *World Neurosurg.* **127**, e261–e267 (2019).
41. Q. Wang, B. Hu, X. Hu, H. Kim, M. Squatrito, L. Scarpace, A. C. deCarvalho, S. Lyu, P. Li, Y. Li, F. Barthel, H. J. Cho, Y.-H. Lin, N. Satani, E. Martinez-Ledesma, S. Zheng, E. Chang, C.-E. G. Sauvé, A. Olar, Z. D. Lan, G. Finocchiaro, J. J. Phillips, M. S. Berger, K. R. Gabrusiewicz, G. Wang, E. Eskilsson, J. Hu, T. Mikkelsen, R. A. DePinho, F. Muller, A. B. Heimberger, E. P. Sulman, D.-H. Nam, R. G. W. Verhaak, Tumor evolution of glioma-intrinsic gene expression subtypes associates with immunological changes in the microenvironment. *Cancer Cell* **32**, 42–56.e6 (2017).
42. R. G. Verhaak, K. A. Hoadley, E. Purdom, V. Wang, Y. Qi, M. D. Wilkerson, C. R. Miller, L. Ding, T. Golub, J. P. Mesirov, G. Alexe, M. Lawrence, M. O'Kelly, P. Tamayo, B. A. Weir, S. Gabriel, W. Winckler, S. Gupta, L. Jakkula, H. S. Feiler, J. G. Hodgson, C. D. James, J. N. Sarkaria, C. Brennan, A. Kahn, P. T. Spellman, R. K. Wilson, T. P. Speed, J. W. Gray, M. Meyerson, G. Getz, C. M. Perou, D. N. Hayes; Cancer Genome Atlas Research Network, Integrated genomic analysis identifies clinically relevant subtypes of glioblastoma characterized by abnormalities in PDGFRA, IDH1, EGFR, and NF1. *Cancer Cell* **17**, 98–110 (2010).
43. C. Neftel, J. Laffy, M. G. Filbin, T. Hara, M. E. Shore, G. J. Rahme, A. R. Richman, D. Silverbush, M. K. L. Shaw, C. M. Hebert, J. Dewitt, S. Gritsch, E. M. Perez, L. N. G. Castro, X. Lan, N. Druck, C. Rodman, D. Dionne, A. Kaplan, M. S. Bertalan, J. Small, K. Pelton, S. Becker, D. Bonal, Q.-D. Nguyen, R. L. Servis, J. M. Fung, R. Mylvaganam, L. Mayr, J. Gojo, C. Haberler, R. Geyeregger, T. Czech, I. Slavc, B. V. Nahed, W. T. Curry, B. S. Carter, H. Wakimoto, P. K. Brastianos, T. T. Batchelor, A. Stemmer-Rachamimov, M. Martinez-Lage, M. P. Frosch, I. Stamenkovic, N. Riggi, E. Rheinbay, M. Monje, O. Rozenblatt-Rosen, D. P. Cahill, A. P. Patel, T. Hunter, I. M. Verma, K. L. Ligon, D. N. Louis, A. Regev, B. E. Bernstein, I. Tirosh, M. L. Suvà, An integrative model of cellular states, plasticity, and genetics for glioblastoma. *Cell* **178**, 835–849.e21 (2019).
44. A. R. Pombo Antunes, I. Scheyltjens, J. Duerinck, B. Neyns, K. Movahedi, J. A. van Ginderachter, Understanding the glioblastoma immune microenvironment as basis for the development of new immunotherapeutic strategies. *eLife* **9**, e52176 (2020).
45. T. Doucette, G. Rao, A. Rao, L. Shen, K. Aldape, J. Wei, K. Dziurzynski, M. Gilbert, A. B. Heimberger, Immune heterogeneity of glioblastoma subtypes: Extrapolation from the cancer genome atlas. *Cancer Immunol. Res.* **1**, 112–122 (2013).
46. A. S. Venteicher, I. Tirosh, C. Hebert, K. Yizhak, C. Neftel, M. G. Filbin, V. Hovestadt, L. E. Escalante, M. K. L. Shaw, C. Rodman, S. M. Gillespie, D. Dionne, C. C. Luo, H. Ravichandran, R. Mylvaganam, C. Mount, M. L. Onozato, B. V. Nahed, H. Wakimoto,

W. T. Curry, A. J. Iafrate, M. N. Rivera, M. P. Frosch, T. R. Golub, P. K. Brastianos, G. Getz, A. P. Patel, M. Monje, D. P. Cahill, O. Rozenblatt-Rosen, D. N. Louis, B. E. Bernstein, A. Regev, M. L. Suvà, Decoupling genetics, lineages, and microenvironment in IDH-mutant gliomas by single-cell RNA-seq. *Science* **355**, eaai8478 (2017).
47. A. P. Patel, I. Tirosh, J. J. Trombetta, A. K. Shalek, S. M. Gillespie, H. Wakimoto, D. P. Cahill, B. V. Nahed, W. T. Curry, R. L. Martuza, D. N. Louis, O. Rozenblatt-Rosen, M. L. Suvà, A. Regev, B. E. Bernstein, Single-cell RNA-seq highlights intratumoral heterogeneity in primary glioblastoma. *Science* **344**, 1396–1401 (2014).
48. A. S. Modrek, D. Golub, T. Khan, D. Bready, J. Prado, C. Bowman, J. Deng, G. Zhang, P. P. Rocha, R. Raviram, C. Lazaris, J. M. Stafford, G. LeRoy, M. Kader, J. Dhaliwal, N. S. Bayin, J. D. Frenster, J. Serrano, L. Chiriboga, R. Baitalmal, G. Nanjangud, A. S. Chi, J. G. Golfinos, J. Wang, M. A. Karajannis, R. A. Bonneau, D. Reinberg, A. Tsirigos, D. Zagzag, M. Snuderl, J. A. Skok, T. A. Neubert, D. G. Placantonakis, Low-grade astrocytoma mutations in IDH1, P53, and ATRX cooperate to block differentiation of human neural stem cells via repression of SOX2. *Cell Rep.* **21**, 1267–1280 (2017).
49. B. Otvos, D. J. Silver, E. E. Mulkearns-Hubert, A. G. Alvarado, S. M. Turaga, M. D. Sorensen, P. Rayman, W. A. Flavahan, J. S. Hale, K. Stoltz, M. Sinyuk, Q. Wu, A. Jarrar, S. H. Kim, P. L. Fox, I. Nakano, J. N. Rich, R. M. Ransohoff, J. Finke, B. W. Kristensen, M. A. Vogelbaum, J. D. Lathia, Cancer stem cell-secreted macrophage migration inhibitory factor stimulates myeloid derived suppressor cell function and facilitates glioblastoma immune evasion. *Stem Cells* **34**, 2026–2039 (2016).
50. J. Sanchez-Ramos, S. Song, V. Sava, B. Catlow, X. Lin, T. Mori, C. Cao, G. W. Arendash, Granulocyte colony stimulating factor decreases brain amyloid burden and reverses cognitive impairment in Alzheimer's mice. *Neuroscience* **163**, 55–72 (2009).
51. B. Li, M. E. Gonzalez-Toledo, C. S. Piao, A. Gu, R. E. Kelley, L. R. Zhao, Stem cell factor and granulocyte colony-stimulating factor reduce β-amyloid deposits in the brains of APP/PS1 transgenic mice. *Alzheimers Res. Ther.* **3**, 8 (2011).
52. L. Dolcetti, E. Peranzoni, S. Ugel, I. Marigo, A. Fernandez Gomez, C. Mesa, M. Geilich, G. Winkels, E. Traggiai, A. Casati, F. Grassi, V. Bronte, Hierarchy of immunosuppressive strength among myeloid-derived suppressor cell subsets is determined by GM-CSF. *Eur. J. Immunol.* **40**, 22–35 (2010).
53. I. Marigo, E. Bosio, S. Solito, C. Mesa, A. Fernandez, L. Dolcetti, S. Ugel, N. Sonda, S. Bicciato, E. Falisi, F. Calabrese, G. Basso, P. Zanovello, E. Cozzi, S. Mandruzzato, V. Bronte, Tumor-induced tolerance and immune suppression depend on the C/EBPbeta transcription factor. *Immunity* **32**, 790–802 (2010).
54. G. J. Baker, M. G. Castro, P. R. Lowenstein, Isolation and flow cytometric analysis of glioma-infiltrating peripheral blood mononuclear cells. *J. Vis. Exp.* **2015**, 53676 (2015).
55. J. F. Curtin, N. Liu, M. Candolfi, W. Xiong, H. Assi, K. Yagiz, M. R. Edwards, K. S. Michelsen, K. M. Kroeger, C. Liu, A. K. M. G. Muhammad, M. C. Clark, M. Arditi, B. Comin-Anduix, A. Ribas, P. R. Lowenstein, M. G. Castro, HMGB1 mediates endogenous TLR2 activation and brain tumor regression. *PLOS Med.* **6**, e10 (2009).
56. N. Kamran, Y. Li, M. Sierra, M. S. Alghamri, P. Kadiyala, H. D. Appelman, M. Edwards, P. R. Lowenstein, M. G. Castro, Melanoma induced immunosuppression is mediated by hematopoietic dysregulation. *Onco. Targets. Ther.* **7**, e1408750 (2018).
57. P. Qiu, E. F. Simonds, S. C. Bendall, K. D. Gibbs Jr., R. V. Bruggner, M. D. Linderman, K. Sachs, G. P. Nolan, S. K. Plevritis, Extracting a cellular hierarchy from high-dimensional cytometry data with SPADE. *Nat. Biotechnol.* **29**, 886–891 (2011).
58. A. Subramanian, P. Tamayo, V. K. Mootha, S. Mukherjee, B. L. Ebert, M. A. Gillette, A. Paulovich, S. L. Pomeroy, T. R. Golub, E. S. Lander, J. P. Mesirov, Gene set enrichment analysis: A knowledge-based approach for interpreting genome-wide expression profiles. *Proc. Natl. Acad. Sci. U.S.A.* **102**, 15545–15550 (2005).
59. E. Z. Macosko, A. Basu, R. Satija, J. Nemesh, K. Shekhar, M. Goldman, I. Tirosh, A. R. Bialas, N. Kamitaki, E. M. Martersteck, J. J. Trombetta, D. A. Weitz, J. R. Sanes, A. K. Shalek, A. Regev, S. A. McCarroll, Highly parallel genome-wide expression profiling of individual cells using nanoliter droplets. *Cell* **161**, 1202–1214 (2015).

Acknowledgments: We thank K. Verbal and A. Gunawan for all the help. We thank the immunology core, UMICH CyTOF core, and the University of Michigan advanced genomic core. **Funding:** This work was supported by National Institutes of Health/National Institute of Neurological Disorders and Stroke (NIH/NINDS) grants (R37-NS094804, R01-NS105556, and R21-NS107894, and Rogel Cancer Center Scholar Award to M.G.C.); NIH/NINDS grants (R01-NS076991, R01-NS082311, and R01-NS096756 to P.R.L.); the Department of Neurosurgery, the Pediatric Brain Tumor Foundation, Leah's Happy Hearts Foundation, Ian's Friends Foundation (IFF), Chad Tough Foundation, Pediatric Brain Tumor Foundation, and Smiles for Sophie Forever Foundation (to M.G.C. and P.R.L.); NIH/NCI T32-CA009676 Post-Doctoral Fellowship (to M.S.A.); and American Brain Tumor Association Basic Research Fellowship "in Memory of Bruce and Brian Jackson" (to M.B.G.-F.). **Author contributions:** M.S.A., P.R.L., and M.G.C. conducted and designed the experiments, analyzed the data, and wrote the manuscript. M.S.A., B.L.M., R.P.A., R.T., C.S.H., S.C., M.V., M.B.G.-F., S.H., A.T., N.K., L.Z., S.M.F., and F.J.N. helped conduct the experiments and data analysis. W.N.A., D.O., J.H., P.G.P., and K.E. provided clinical patient samples and patient information. S.H.-J. provided glioma patient–derived cells. S.D.M. and G.N. assisted with study design and analysis. P.J.U., J.W., C.G., and J.L. assisted with the single-cell RNA sequencing analysis. D.H. donated the glioma mouse models using the RCAS system. P.R.L. and M.G.C. directed the research and generated the funding. All authors read and edited the manuscript. **Competing interests:** The authors declare that they have no competing interests. **Data and materials availability:** All data needed to evaluate the conclusions in the paper are present in the paper and/or the Supplementary Materials. The RNA-seq and sc-RNA-seq datasets have been deposited in NCBI's Gene Expression Omnibus with identifiers GSE152277. CyTOF data are deposited in Immport (accession number: SDY1774). All plasmids described in this study have been deposited in Addgene (table S6). Further information and requests for resources and reagents should be directed to and will be fulfilled by the corresponding author, MGC (mariacas@med.umich.edu).

Submitted 1 March 2021
Accepted 6 August 2021
Published 29 September 2021
10.1126/sciadv.abh3243

Citation: M. S. Alghamri, B. L. McClellan, R. P. Avvari, R. Thalla, S. Carney, C. S. Hartlage, S. Haase, M. Ventosa, A. Taher, N. Kamran, L. Zhang, S. M. Faisal, F. J. Núñez, M. B. Garcia-Fabiani, W. N. Al-Holou, D. Orringer, S. Hervey-Jumper, J. Heth, P. G. Patil, K. Eddy, S. D. Merajver, P. J. Ulintz, J. Welch, C. Gao, J. Liu, G. Núñez, D. Hambardzumyan, P. R. Lowenstein, M. G. Castro, G-CSF secreted by mutant IDH1 glioma stem cells abolishes myeloid cell immunosuppression and enhances the efficacy of immunotherapy. *Sci. Adv.* **7**, eabh3243 (2021).